FACULTY OF ENGINEERING AND TECHNOLOGY

DEPARTMENT OF WATER RESOURCES ENGINEERING

FINAL YEAR PROJECT

DESIGN AND CONSTRUCTION OF A WATER SOFTENING SYSTEM

CASE STUDY: LOGIN HOSTEL (SYAULE)

BY

MASENGERE ISAAC GRACE

BU/UP/2022/1707

SUPERVISOR: MR. MASERUKA BENDICTO

A final year project report presented to the Department of Water Resources Engineering as partial fulfillment of the requirements for the award of a Bachelor of Science in Water Resources Engineering of Busitema University.

APRIL 2026

ABSTRACT

Access to clean, safe, and readily available drinking water is a fundamental pillar of public health and sustainable development worldwide. The borehole supplying Login Hostel in Syaule, Busia District, has severely hard water (320 mg/L as CaCO3), causing health and operational problems for students. To solve this, we designed and built a solar-powered electrocoagulation water softening system. The system meets a maximum daily demand of 3.9 m3/d for 30 residents. Electrocoagulation was chosen because it scored highest (126 points) in a technology analysis, and aluminum was selected for both electrodes with a score of 135 points. The design features a 7-ring helical coil creating 6 electrochemical cells inside a 3.5-inch polyvinyl chloride casing. It includes a three-stage downstream filter: a polypropylene sediment filter, a granular activated carbon buffer, and a compressed carbon block. Power comes from a 12.8 V, 120 Ah LiFePO4 battery, charged by a 300 W to 350 W monocrystalline solar panel and regulated by a 30 A Maximum Power Point Tracking charge controller.

Testing at 9 V, 12 V, and 24 V proved that 12 V works best. At 12 V, the system removed 62% of the water hardness while using only 0.81 kWh/m3 of electricity. After 60 minutes of continuous flow, the final hardness dropped to a safe 125.3 mg/L. A 24-hour test showed the battery stayed safely above a 50% charge level throughout operation. Financially, the system costs 1,200,000 Ugandan Shillings to build. Over five years, it produces a Net Present Value of 11,330,586 Ugandan Shillings, a payback period of 5.4 months, and a profitability index of 7.30.

Keywords: Electrocoagulation; Hard Water; Water Softening; Aluminum Electrodes; LiFePO4 Battery; Solar Photovoltaic; Faraday's Law; Hardness Removal Efficiency

DECLARATION

I, MASENGERE ISAAC GRACE, hereby certify that the content in this report was created by me using my own time and the knowledge and that it has never been shared with a business or organization. I assume complete responsibility for it.

Date: 08/06/26

Signature: 

Email: masengereisaac911@gmail.com

Tel No: 0752030201 / 0761568885

APPROVAL

This report has been submitted to the Faculty of Engineering for examination with approval of my supervisor.

Mr. Maseruka S. Bendicto

ACKNOWLEDGEMENT

I truly thank God for giving me the health, wisdom, and strength to complete this work.

I also thank my parents, for the constant love, support, and encouragement which have been my motivation throughout my studies.

I also appreciate the opportunity to work with Busitema university and the authority of Login hostel which is my study area, for allowing me to access the water facilities often for carrying out my project and I am indeed thankful for the valuable resources and information they provided which were very important for this project's success.

I want to give a special thanks to my supervisor, Mr. Maseruka S. Bendicto, for his expert guidance, helpful feedback, and patience that helped shape this work.

Lastly, to my course mates, thank you for your friendship and for making my time at university a great experience.

LIST OF FIGURES

LIST OF TABLES

LIST OF ACRONYMS

APHA	American Public Health Association
AWWA	American Water Works Association
BoQ	Bill of Quantities
CFU	Colony Forming Units
CT	Contact Time
DPD	Diethyl-p-phenylene diamine
DPP	Discounted Payback Period
EC	Electrical Conductivity
EDTA	Ethylenediaminetetraacetic acid
HDPE	High-Density Polyethylene
IIC	Initial Investment Cost
IRR	Internal Rate of Return
MWE	Ministry of Water and Environment
NDP IV	National Development Plan IV
NF	Nanofiltration
NPV	Net Present Value
NRW	Non-Revenue Water
NTU	Nephelometric Turbidity Units
NWSC	National Water and Sewerage Corporation
RO	Reverse Osmosis
SDG 6	Sustainable Development Goal 6
TSS	Total Suspended Solids
U.S. EPA	U.S. Environmental Protection Agency

WEF Water Environment Federation

Table of Contents

CHAPTER 1 INTRODUCTION

1.1 Background

Having access to clean, safe, and easily available drinking water is a foundation of public health, economic growth, and city development (UNICEF, 2023). Globally, about 27% of people did not have access to safely managed drinking water in 2022 meaning, 2.2 billion people, still do not have this basic need met, showing a serious and ongoing problem (WHO, 2023). In 2019 alone, poor water, sanitation, and hygiene were linked to about 1.4 million deaths and 74 million years of healthy life lost worldwide (Zyoud & Zyoud, 2023). In Bangladesh, about 30 million people are exposed to arsenic in their drinking water at levels higher than 10 µg/L. (Paul et al., 2022). Even developed nations face issues, as seen in a 2024 incident near Brixham, England, where parasite contamination led to a long-term boil-water notice for around 17,000 homes and businesses (South West Water, 2024).

In Africa, Kenya had 12,120 cholera cases and 202 deaths between October 2022 and October 2023. Malawi's cholera outbreak in 2022-2023 caused 58,982 cases and 1,771 deaths. The World Health Organisation (WHO) reported over 708,200 cases of cholera or similar illnesses and 4,300 deaths in 2023 (WHO, 2024). Studies in countries like Ghana and Niger found that many stored drinking water samples had more than 11 Colony Forming Units (CFU)/100ml, which is far above the safe limit of zero (Onda et al., 2019). A wider study showed that 87% of water sources in Kabarole had E.coli, making them unsafe to use without treatment (Aquaya, 2024). Lab tests in Mbarara City showed that 55.5% of E.coli from water sources were resistant to the antibiotics, making infections harder and more expensive to treat (IWA Publishing, 2024).

The failure of water treatment systems in some of these areas especially the rural areas is as a result of several factors, starting with the general lack of awareness on treatment treatment and knowledge to properly operate and maintain the installed systems (Olympian Water Testing, 2023). This is compounded by inadequate funding , where the high operational costs for monitoring and repairs are unaffordable for many

communities (Camero et al., 2023). Furthermore, the absence of reliable and affordable energy sources presents a significant barrier, particularly for systems requiring electricity or heating for the treatment process (Moerk Water, 2025; Plappally, 2025). Inadequate initial planning, which fails to select technology appropriate for local conditions, also contributes significantly to the failure of these essential systems (Plizma Technology, 2025)

Different water treatment methods have worked well around the world when they are used and maintained correctly. In Peru, a solar-powered plant that used sedimentation, oxidation, and adsorption was very effective, removing 99.72–99.85% of arsenic and leaving less than 0.01 mg/L. It also reduced cloudiness in the water by up to 66.7% (Mori Sosa et al., 2025). In Sri Lanka, reverse osmosis (RO) stations worked well, removing about 95.8% of water hardness and reducing alkalinity by around 86.6%. In Nigeria, ceramic filters made with burnt sawdust or maize-cobs removed about 70.4 to 75.6% of cloudiness by the fifth week and lowered calcium and magnesium by about 57 to 59%, which makes the water less hard (Bulta & Micheal, 2019).

In Uganda, at Kampala's Ggaba I plant, a direct dual-media filter using anthracite and sand with a coagulant chemical lowered the cloudiness from 8 NTU down to about 0.7 NTU and achieved 0 mg/L of total suspended solids. This method was expected to increase the plant's water production by 23.6%, which is important for the growing city population (Nakimuli, 2021). At the Ggaba III plant, putting shelters over the clarifiers and filters greatly reduced algae (by about 96.6%) and lowered the cloudiness of the filtered water by about 87.9%.

The water supply system at Login Hostel , installed in 2025, is set up an electric-powered boreholes that pump water into a large a 1000 litre storage tank through a 1-inch pipe. This area's bore holes have been characterised by hard water.

1.2 Problem statement

Unsafe drinking water remains a critical global health crisis affecting billions, a problem mirrored by the challenges faced globally (WHO, 2023).Syaule faces water scarcity and supply issues stemming from aging boreholes. These supply challenges are

complemented by poor water quality, which includes high levels of hardness which pose risk to the community and necessitate an effective treatment system. Various solutions have been practiced towards water quality around Syaule in Busitema parish such as Kalende et al., (2024) a Busitema university student who constructed a chlorination system which only covers Njuki Girls' hostel, leaving the rest of the facilities like boys' halls of residence, faculty building and restaurant uncatered for. The direct consequence of using untreated hard water is a continuous domestic and economic burden, leading to severely clogged plumbing, damaged water-heating appliances, and excessive soap consumption, ultimately affecting the living costs and daily comfort of communities like the one at Login Hostel (Shayo et al., 2023).

1.3 Justification

If the untreated hard water problem is not fixed at Login Hostel, we are heading for an infrastructural and environmental disaster. The high mineral content will eventually destroy our plumbing systems and water heaters, as it causes severe internal scaling. This scaling not only ruins the appliances but requires significantly more electrical energy to heat and boil water, driving up utility costs and creating potential fire or breakdown hazards. Because the untreated hard water tastes highly metallic and leaves a chalky residue, students are forced to rely entirely on bottled water for drinking. This creates a huge plastic trash problem at the hostel and gives it terrible reputation for basic student care and sustainability. Furthermore, continuous exposure to untreated hard water can cause widespread dermatological issues, such as severe dry skin, scalp irritation, and eczema flare-ups (Lanrewaju et al., 2022) among students and other residents. Ultimately, the progressive destruction of the building's pipes and overwhelming student complaints could lead to costly emergency maintenance and force the hostel to temporarily shut down.

1.4 Main objective

To design and construct a water softening system .

1.5 Specific objectives

To design the components of the softening system

To construct the water softening system.

To test the performance of the water softening system.

1.6 Research Questions

What are the optimal design parameters and specifications for the water softening system components to ensure effective water treatment?

What are the most suitable materials and construction methodologies for a durable and efficient water softening system?

How effective is the constructed system at removing contaminants, and does it meet the required water quality standards?

1.7 Significance

This study aims to design and build a water softening system at Login Hostel. This project will directly benefit students by providing soft water that tastes better, makes washing clothes easier, and stops dry skin and hair problems. The university administration will also save money because soft water stops hard minerals from blocking pipes and destroying water heaters, which lowers repair costs. The main result will be a fully working water softening plant that gives a reliable supply of good quality water. This project supports Sustainable Development Goal 6 (SDG 6) by improving water quality for everyone. It also matches Uganda's National Development Plan IV (NDP IV) by improving basic student services and keeping students comfortable and productive.

1.8 Scope

This project aims towards the design and construct a water treatment system for Login hostel, focusing specifically on softening, and filtration to improve water quality. The scope is confined to treating the primary water source for issues of hardness, and

suspended solids. It will not consider the removal of complex chemical contaminants like heavy metals or the complete overhaul of the existing campus-wide distribution network. This project will be completed in a period of 3 months.

CHAPTER 2 LITERATURE REVIEW

2.1 Introduction

This chapter presents a detailed review of existing literature concerning continuous problems associated with hard water, the natural causes of its occurrence in groundwater, its broad health and economic effects, and the diverse treatment technologies used to mitigate it. In addition to a thorough exploration of six conventional and emerging water softening technologies, this chapter provides a specific focus on electrodialysis. Furthermore, the principles of electrochemical reactions, reactor design parameters, and the strategic integration of solar photovoltaic (PV) systems to power these sustainable water treatment technologies are evaluated. The overarching aim of this review is to build a robust, higher-level academic foundation for the methodology of this study.

2.2 Hard Water Characterization

2.2.1 Causes of Hardness in Groundwater

Groundwater naturally interacts with the Earth's geosphere, dissolving a variety of minerals as it percolates through soil and rock boundaries. Hardness in groundwater is principally caused by the dissolution of multivalent metallic cations, predominantly calcium (Ca^{2+}) and magnesium (Mg^{2+}) ions (World Health Organization [WHO], 2022). The primary geological sources of these ions are sedimentary rocks, such as limestone (calcite, $CaCO_3$) and dolomite ($CaMg(CO_3)_2$), which slowly dissolve when exposed to slightly acidic rainwater carrying dissolved carbon dioxide (Patel & Smith, 2023). Furthermore, the presence of gypsum (calcium sulfate dihydrate, $CaSO_4 \cdot 2H_2O$) in underground rock formations contributes to non-carbonate or "permanent" hardness, which is generally more difficult to remove than carbonate hardness (Davies & White,

2021). As a result, regions heavily dominated by these specific geological formations naturally feature groundwater sources with highly elevated water hardness levels.

2.2.2 The Effects of Hard Water

The persistent use of hard water results in significant domestic, industrial, health-related, and economic impacts. One of the most common physical effects is the formation of insoluble precipitates (scale), such as calcium carbonate, inside household pipes, boilers, and heat exchangers when the water is heated (Johnson et al., 2021). This scaling restricts water flow and drastically reduces the energy efficiency of water heating devices, eventually leading to costly mechanical failures and replacements. Furthermore, the calcium and magnesium ions in hard water interact with the fatty acids in standard soaps and detergents to form a scummy residue instead of lather, forcing households to use larger quantities of chemical cleaning agents, which increases environmental pollution downstream (Wang & Zhou, 2024). Although the World Health Organization states there is no direct, severe health risk from drinking moderately hard water, overly high mineral concentrations can negatively impact the taste of water and may aggravate skin conditions such as eczema in susceptible individuals (WHO, 2022).

2.3 Technology Development (Softening Methods)

To address the diverse challenges of hard water, numerous technologies have been engineered to remove or neutralize the responsible ions. While this study focuses on electrodialysis as a primary application, six other prominent technologies have been widely used globally in both municipal and domestic applications to achieve reliable water softening.

2.3.1 Ion Exchange Water Softening

Ion exchange is the most widely adopted method for domestic water softening. According to Miller and Brown (2022), the process works by passing the hard water through a vessel filled with synthetic, negatively charged resin beads that are pre-coated with sodium (Na^+) or potassium (K^+) ions. Due to their higher charge and affinity, the calcium and magnesium ions forcefully displace the sodium ions and attach themselves to the resin beads. The resulting softened water is infused with the displaced sodium

ions. While highly effective, this conventional method introduces the environmental problem of discharging concentrated brine (saltwater) back into the ecosystem whenever the resin must be regenerated and cleaned (Johnson et al., 2021).

2.3.2 Lime-Soda Ash Chemical Softening

Often used in large-scale municipal water treatment plants, the lime-soda ash method involves adding calculated amounts of slaked lime (calcium hydroxide) and soda ash (sodium carbonate) directly into the hard water (Davis & Miller, 2022). This chemical addition instantly increases the water's pH and forces the soluble calcium and magnesium ions to precipitate out of the solution entirely as solid calcium carbonate and magnesium hydroxide (Ogunbiyi & Peters, 2020). While economically feasible for massive bulk volumes of water, the resulting physical process generates a massive amount of wet, solid sludge that strictly requires specialized disposal protocols, rendering it impractical for small-scale operations.

2.3.3 Reverse Osmosis (RO) Membrane Filtration

Reverse Osmosis serves as an intensive physical separation technology. The method involves placing the source water under exceptionally high mechanical pressure to force the water molecules through a semi-permeable microscopic membrane, leaving almost all dissolved salts, including hardness ions, trapped behind (Lee & Park, 2024). Although RO yields water of the highest purity possible, it demands significant electrical energy to maintain the necessary pressure. Moreover, it is notorious for rejecting large fractions of the input water as brine waste, which reduces total water conservation efficiency for ordinary softening purposes (Singh et al., 2021).

2.3.4 Nanofiltration (NF)

Similar to reverse osmosis but operating at a slightly lower mechanical pressure with slightly larger membrane pores, nanofiltration is specifically tailored to selectively reject large multivalent ions like calcium, magnesium, and sulfates, while allowing smaller monovalent ions to pass freely (Zhao & Chen, 2025). According to Kamaraj et al. (2019), nanofiltration successfully bridges the gap between ultrafiltration and reverse osmosis. It provides highly efficient water softening but suffers from gradual membrane

degradation and requires strict pretreatment to prevent the membrane from prematurely fouling due to scaling.

2.3.5 Capacitive Deionization (CDI)

Capacitive Deionization is a rapidly emerging electrochemical technology that removes charged ions by applying a low-voltage electrical field across a pair of highly porous carbon composite electrodes (Choi et al., 2023). As the hard water flows through the defined cell, the calcium and magnesium cations are electrostatically pulled toward and trapped entirely within the porous structure of the negatively charged cathode. When the electrodes reach their specific saturation limit, the electrical polarity is fully reversed, repelling the captured ions into a concentrated waste stream (Zhang & Wu, 2022). Although extremely energy-efficient, CDI is currently constrained by the high production costs of the carbon aerogel electrodes.

2.3.6 Template Assisted Crystallization (TAC)

Unlike traditional removal systems, Template Assisted Crystallization acts purely as an advanced physical scale inhibitor rather than a direct ion remover. In this approach, hard water interacts with specialized polymeric beads inside a media tank. The surface of these beads features distinct nucleation templates that force the dissolved calcium and magnesium ions to instantly crystallize into harmless, microscopic, stable crystals (Fox & Taylor, 2021). Because these new microscopic crystals remain in suspension, they pass freely through pipes without ever sticking to surfaces or forming scale (Adams & Clark, 2024). This system is exceptionally low maintenance and salt-free, yet it does not physically lower the measurable hardness level of the water.

2.4 Environmental and Solar Sizing Effects on Treatment Performance

2.4.1 Electrodialysis and Electrochemical Reactions

Among the advanced, sustainable water treatment tools, electrochemical methods perfectly utilize direct electrical currents to trigger specific chemical transformations directly inside the hard water matrix. In electrodialysis using consumable, sacrificial electrodes like aluminum, the system efficiently initiates a controlled liberation of

metallic ions directly into the aqueous solution (Moussa et al., 2021). The targeted reaction at the active anode oxidizes the aluminum, while the cathode simultaneously reduces the surrounding water molecules to produce hydrogen gas and highly reactive hydroxyl ions (OH^-). This rapid surge of hydroxyl ions quickly raises the localized pH adjacent to the cathode, forcing dissolved calcium and magnesium to spontaneously precipitate into insoluble calcium carbonate ($CaCO_3$) and magnesium hydroxide ($Mg(OH)_2$) (Garcia-Segura et al., 2022). This distinctive process ultimately ensures highly efficient physical hardness removal without requiring frequent additions of external chemical reagents.

2.4.2 Reactor Design, Operational Parameters, and Material Selection

The total operational efficiency of any electrochemical softening system natively relies heavily on the physical geometric properties of its continuous-flow reactor and its operating settings. The efficiency of electrocoagulation and electrodialysis for water softening is profoundly influenced by the precise relationship between applied voltage, current, retention time, electrode spacing, hardness concentration, and the specific material selection for the electrodes (El-Taweel et al., 2023).

Voltage, Current, and Retention Time:

The applied voltage and current density directly control the rate of coagulant dosage generation (e.g., Al^{3+} or Fe^{2+} ions) and the magnitude of localized pH shifts (Devlin et al., 2019). Higher current densities typically accelerate the precipitation of hardness ions, but excessively high currents waste energy through parasitic reactions such as excessive oxygen evolution and accelerated electrode passivation. The hydraulic retention time (HRT) works in tandem with current; a longer retention time allows sufficient contact between the hardness ions and the generated coagulants or hydroxyl ions, ensuring complete crystallization and agglomeration, whereas too short an HRT may lead to incomplete softening (Sardari et al., 2020).

Electrode Spacing and Hardness Concentration:

The inter-electrode spacing is a crucial geometrical parameter. Narrowing the spacing between the activated anode and cathode reliably minimizes the electrical resistance of

the water (IR drop), thereby substantially dropping the overall power requirement necessary to continuously run the reactor (Yiga et al., 2023). However, if the spacing is too narrow, precipitated scale ($CaCO_3$ and $Mg(OH)_2$) can bridge the gap, causing electrical short circuits and restricting fluid flow. The initial hardness concentration also heavily dictates these parameters; highly hard water inherently provides higher electrical conductivity, facilitating current flow at lower voltages, but requires proportionally higher current inputs and longer retention times to fully precipitate the massive quantities of dissolved calcium and magnesium (El-Taweel et al., 2023).

Material Selection of Electrodes:

The choice of metallic material for the several electrodes is arguably the most critical constraint in electrocoagulation. Aluminum and iron are the most universally utilized sacrificial anodes due to their high electrochemical equivalent, availability, and low cost. Aluminum anodes dissolve to form highly effective polymeric aluminum hydroxide complexes that sweep up precipitated hardness scale, making them highly efficient for combined softening and clarification (Moussa et al., 2021). Iron electrodes, while effective, can leave residual colors in the treated water. For the cathode, inert materials such as stainless steel, titanium, or graphite are frequently employed because they resist degradation over time and efficiently facilitate the reduction of water into hydrogen gas and the critical hydroxyl ions needed to drive hardness precipitation without adding additional trace metals to the water (Liu et al., 2022). By mathematically applying Faraday's Law of Electrolysis, scientists can directly simulate the accurate amount of real electrical current and time inherently required to dissolve the proper stoichiometric mass of the selected electrode material for comprehensive ion removal (ALRubaye et al., 2024).

2.4.3 Solar-Powered Water Treatment System Sizing

Effectively implementing functional water treatment innovations inside remote or entirely off-grid rural regions invariably necessitates an independent, highly reliable, and renewable energy foundation. Modern solar photovoltaic (PV) modular arrays afford an exceptionally clean and robust pathway to sustainably power small-scale

electrochemical reactors (Subramanian et al., 2021). Because fundamental electrodialysis purely requires a direct current (DC) input, it organically merges with basic solar panels and deep-cycle battery storage networks without depending on any fragile or complex power inversion systems (Sen et al., 2019). Careful system sizing entails accurately matching the daily power load of both the active reactor and its circulation pump with the unique localized daily solar irradiation statistics, ensuring enough continuous battery backup exists to bridge multiple cloudy spans uninterrupted (Kumar & Raja, 2020). Seamlessly integrating solar technology with dedicated electrochemical softening successfully forms a lasting, socially accessible solution for the treatment of persistently hard water.

CHAPTER 3 METHODOLOGY

This chapter explains the steps taken to design and build the water treatment system. The steps match the main project objectives.

3.1 Case Study Description and Site Location

This case study focuses on Login Hostel in Syaule, a small community located in the Busitema area of Busia District in Eastern Uganda. The village is easy to reach because it sits just off the main highway. It is located about 25 kilometers away from Busia town, which is the main commercial town near the border of Uganda and Kenya (UBOS, 2021).

In Syaule, people do not have access to large rivers or piped tap water. Instead, the major source of water for the entire area is groundwater (MWE, 2023). Families, hostels, and schools get their daily water by pumping it out of deep boreholes and wells. Because this water sits deep underground, it mixes with the natural rocks and soils. This causes the water to absorb high amounts of dissolved minerals, which is the main reason why the groundwater in this region is very hard (Wandera et al., 2022).

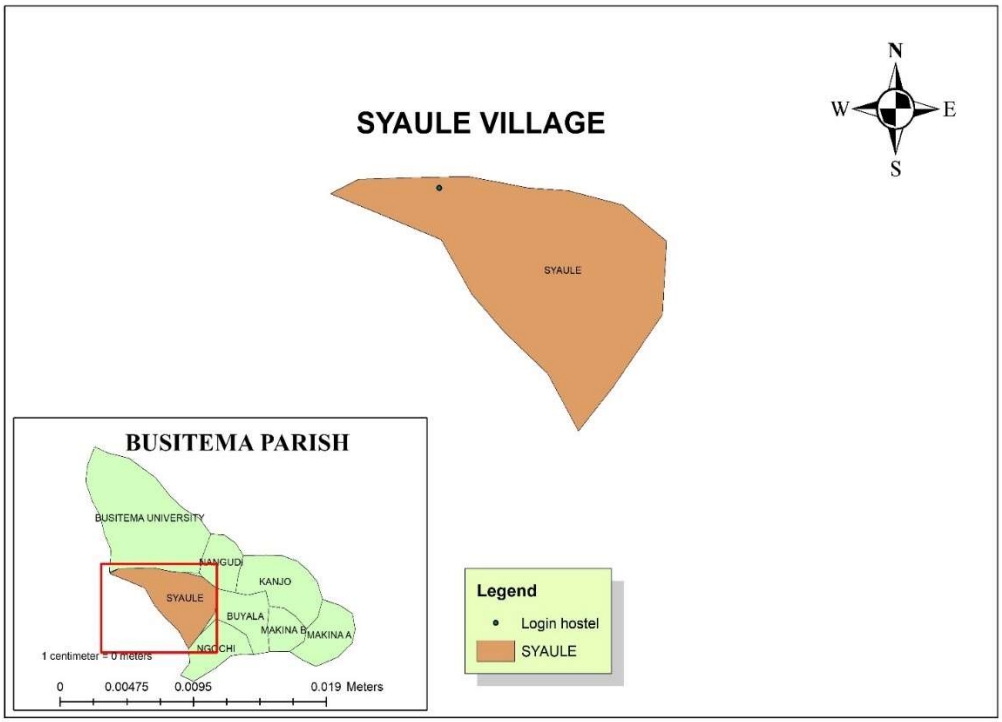

Figure 3.1:A map showing location of Login Hostel

Figure 2: Student collecting a water sample at the case study borehole (fore ground) at login hostel (in the back ground

3.2 Water Demand Estimation

To determine the capacity of the proposed treatment and distribution system, the total water demand was calculated based on the standards provided in the MWE Water Supply Design Manual (2013). The methodology involves establishing the design population and applying per capita consumption rates.

3.2.1 Design Population (P_d)

The design population represents the total number of users the system is intended to serve. For this study, the population is fixed based on the hostel's capacity as shown in equation (3.1).

$$P_d = P_{res} \tag{3.1}$$

Where P_d is the Total design population (persons) P_{res} Number of permanent residents

3.2.2 Unit Water Demand (q)

The unit demand is the volume of water allocated per person per day. According to the MWE (2013) manual, for boarding institutions (hostels) equipped with Water Closets (WC), a standard demand of 100 l/c/d is adopted.

Average Daily Demand (ADD)

The ADD is the total daily water requirement for the entire population under normal conditions. It is calculated by multiplying the design population by the unit demand as shown below in Equation (3.2)(*MWE*, 2013).

$$ADD\ (m^3/d)\ =\ \frac{(Pd\ \times\ q)}{1000} \tag{3.2}$$

Where: ADD is Average Daily Demand (m^3/d) and q is Per capita water demand (100 l/c/d)

Peak Demand Factors

Water consumption fluctuates throughout the day and year. To ensure the system can handle these variations, peak factors are applied as per (MWE, 2013).

Maximum Daily Demand (MDD): Accommodates the day with the highest consumption. A peak day factor (k_1) of 1.3 is applied as shown in equation (3.3) below.

$$MDD\ =\ ADD\ \times\ k_1 \tag{3.3}$$

Peak Hourly Demand (PHD): Determines the maximum flow rate during the busiest hour. A peak hour factor (k_2) of 2.0 is used as shown in equation (3.4) (*MWE*, 2013)below.

$$PHD\ =\frac{(MDD\ \times\ k_2)}{24} \tag{3.4}$$

3.3 Sampling Criteria and Water characterisation

To accurately assess groundwater conditions and establish a reliable baseline for the water treatment system, samples were collected four times over a month to capture

environmental variations (APHA, 2023; AWWA, 2023; WEF, 2023). The process began with careful site cleaning and measuring water depth to calculate the required purge volume. Stagnant water was then removed at a slow speed while monitoring temperature, pH, and electrical conductivity until three consecutive readings stabilized, guaranteeing the collection of fresh groundwater (APHA, 2023; AWWA, 2023; WEF, 2023).

Following stabilization, water was carefully pumped into completely filled lab bottles to prevent air exposure and chemical alteration. The bottles were securely capped, labeled with required tests like Total Hardness, and treated with nitric acid to preserve dissolved metals. They were immediately stored in coolers packed with ice along with a temperature blank to halt bacterial growth and chemical shifts (APHA, 2023; AWWA, 2023).

Complete paperwork and detailed field notes accompanied the samples, which were safely transported to the laboratory within four days. Establishing these raw water baselines through standard APHA methods is critical for accurately designing the physical and electrical components of the treatment system (Sardari et al., 2020)

3.3.1 Determination of Hydrogen Ion Concentration (pH)

The pH dictates the predominant speciation of dissolved aluminum (e.g., $Al(OH)_3$) and directly impacts anodic dissolution kinetics (Garcia-Segura et al., 2022). First, the test used a Hach HQ40d Portable Meter with a pH sensor, a magnetic stirrer, and clean 500 mL glass cups. Before testing, the pH sensor was checked using standard solutions (pH 4.0, 7.0, and 10.0) to make sure it read right. Then, a 200 mL sample of the raw groundwater was poured into the cup and placed on the magnetic stirrer, mixed gently to make the water even. Finally, the clean pH sensor was fully dunked into the water without touching the cup's sides. The screen reading was left to settle and recorded once the temperature was steady (APHA, 2023; AWWA,2022).

3.3.2 Determination of Electrical Conductivity (EC)

EC controls how easily electricity flows through the water between the metal coils. This is a very important number for figuring out the reactor's power needs (Sen et al., 2019).

The same portable meter was used, but with a different sensor attached for testing conductivity. The sensor was tested first using a known salt solution. It was washed with clean distilled water and dried before use. The sensor was put all the way into a cup of gently stirred water. The worker tapped the sensor to knock off any trapped air bubbles, which can cause a bad reading. Once the screen showed a steady number at 25°C, the exact EC value was written down (APHA, 2023; AWWA,2022).

3.3.3 Determination of Total Hardness

Finding the total hardness (the amount of calcium and magnesium) helps calculate the exact power and time needed to soften the water (Subramanian et al., 2021; ALRubaye et al., 2024). The test needed a very exact measuring tube (burette) on a stand, glass flasks, glass pipettes, and a magnetic stirrer over a white background. The needed chemicals were a standard EDTA mixture, an ammonia buffer, and EBT colour powder. Exactly 50 mL of the hard water was moved into the glass flask. A small amount of ammonia was added to hold the water's pH exactly at 10.0, so the colour test would work perfectly. A small scoop of the EBT colour powder was added and mixed, turning the water a dark red colour. While stirring, the EDTA mixture was dripped into the flask one drop at a time. The EDTA catches and holds onto the calcium and magnesium. The test stopped the second the water lost all red colour and turned bright blue. The total hardness was calculated using the exact amount of EDTA dripped (APHA, 2023; AWWA, 2023; WEF, 2023).

Figure 3.3:Scaling formed on the heating coil due to hard water

Figure 3.4:Carrying out EDTA test to determine hardness of the raw borehole water

3.4 Selection Water Softening Method and Electrodes

3.4.1 Softening Method Selection Criteria

A scoring table was made to pick the best water softening method for the project. Four common ways were compared: Ion Exchange, Lime-Soda Ash Softening, Reverse Osmosis, and Electrodialysis.

Seven points were used to compare the methods, matching exactly what the project needed. These points are: starting cost, power needed, running limits and fixing costs, how well it works, needed skills, easy to find items, and space taken.

A weight heavily from 1 to 5 is given to each point based on how much it helps the project. A weight of 5 means the point is very helpful, while a weight of 1 means it is not very helpful. The weights were set based on project goals like keeping costs low, easy running, and using local things. Starting cost has a weight of 4, meaning it is very helpful because a lower setup cost is great when there is little money. Power needed has a weight of 3, meaning it is somewhat helpful since some power can be supported by solar. Running and fixing cost has a weight of 5, making it the most helpful because low daily and fixing costs give the biggest help to keep the project going. How well it works also has a weight of 5 because strong hardness removal guarantees the best water. Needed skills and easily found items both have a weight of 4, which is very helpful because not needing special training means locals can easily run it, and easy to get items make the supply simple. Lastly, space taken has a weight of 3, as a smaller size makes it fit better.

Every method was given a base score from 1 to 5 on every point based on how well it helped. A score of 5 means the method is the best for that point (for example, a 5 on starting cost means it has the lowest price, and a 5 on how well it works means it takes out the most hardness). The total points are found by multiplying the assigned weight by the method's base score. All points are added up to find the total score. The method with the biggest total score is picked. The scoring table is shown below (Table 3.1). The numbers in brackets show the final points (weight × score).

Table 3.1:Showing selection of methods

Method	Initial cost(wt 4)	Power req(wt 3)	O&M cost(wt 5)	Efficiency(wt 5)	Expertise(wt 4)	Materials (wt 4)	Space (wt 3)	Total score
Ion exchange	3 (12)	5 (15)	3 (15)	5 (25)	4 (16)	4 (16)	3 (9)	108
Lime-soda ash softening	5 (20)	5 (15)	2 (10)	4 (20)	3 (12)	5 (20)	2 (6)	103
Reverse osmosis	2 (8)	2 (6)	2 (10)	5 (25)	2 (8)	3 (12)	4 (12)	81
Electrodialysis	4 (16)	3 (9)	5 (25)	5 (25)	4 (16)	5 (20)	5 (15)	126

Electrodialysis gets the biggest total score of 126. This method is picked for the project. It has very low running and fixing costs because no extra chemicals are needed, and there is very little waste. It works very well to take out hardness, and uses metal parts that are easy to find and replace nearby. Also, the system takes up little space and needs only basic skills to run. These points make electrodialysis better than the other ways to soften well water. It perfectly fits the project needs for a easy, low-cost, and lasting system.

3.4.2 Electrode Material Selection Criteria

Another scoring table was made to pick the best metals for the electrodialysis parts. Eight common metals were checked: aluminium, mild steel, iron, graphite, stainless steel, copper, titanium, and zinc.

Seven points were used to compare the metals, matching exactly what the project needed to treat the well water. The points are: metal price, easy to find, how good it is at taking out hardness, how it acts in the water with power, how well it moves power, how long it lasts, and if it is safe for the area.

A weight heavily from 1 to 5 was given to each point based on how helpful it is for the project. A weight of 5 means the point is very helpful, while a weight of 1 means not very helpful. The weights were set like this to meet project goals like low price, easy to buy nearby, and good hardness removal. Metal price and easy to find both have a weight

of 5, as low price keeps the project cheap and easy to buy nearby stops delays. How good it removes hardness also has a weight of 5, making it the most helpful since taking out calcium and magnesium is the main goal. Reaction with power has a weight of 4, which is very helpful because breaking down well creates strong cleaners in the water. Moving power has a weight of 3, meaning it is somewhat helpful to use less power. How long it lasts and being safe for the area both have a weight of 4, making them very helpful because lasting longer means buying replacements less often, and safe metals keep the clean water safe.

Every metal was given a score from 1 to 5 on every point based on how well it helped. For example, a score of 5 on metal price means it is the cheapest, and a score of 5 on hardness removal means it takes out the most calcium and magnesium. The final points for each unit are found by multiplying the assigned weight by the metal's score. The table shows the base score followed by the final points in brackets. The total score is all the final points added together. The scoring table is shown below in Table 3.2, telling which metal is best for the positive side (anode) or negative side (cathode).

Table 3.2:sowing Selection of Electrode material.

Material	Cost (wt 5)	Avail. (wt 5)	Efficiency (wt 5)	Reaction (wt 4)	Conduct. (wt 3)	Durability (wt 4)	Safety (wt 4)	Best for	Total
Aluminium	5 (25)	5 (25)	5 (25)	5 (20)	4 (12)	3 (12)	4 (16)	Anode	135
Mild steel	5 (25)	5 (25)	4 (20)	5 (20)	4 (12)	3 (12)	3 (12)	Anode	126
Iron	5 (25)	5 (25)	4 (20)	5 (20)	4 (12)	3 (12)	3 (12)	Anode	126
Graphite	4 (20)	3 (15)	3 (15)	1 (4)	5 (15)	5 (20)	5 (20)	Cathode	109
Stainless steel	3 (15)	4 (20)	4 (20)	2 (8)	4 (12)	5 (20)	5 (20)	Cathode	115

Copper	2 (10)	3 (15)	2 (10)	4 (16)	5 (15)	2 (8)	1 (4)	Anode	78
Titanium	1 (5)	2 (10)	4 (20)	3 (12)	4 (12)	5 (20)	4 (16)	Cathode	95
Zinc	4 (20)	3 (15)	3 (15)	4 (16)	4 (12)	2 (8)	2 (8)	Anode	94

Aluminium gets the highest total score of 135. These two metals are chosen for the project. Aluminium is used as both the positive side (anode) and as the negative side (cathode) (Garcia-Segura et al., 2022). Aluminium is picked for the both positive and negative electrode because it works the best for taking out hardness. It breaks down in the water to make clumps that physically catch calcium and magnesium very well. It is also cheap, easy to find, and works very well with power. These points make it much better than iron or mild steel (which add too much waste and rust colour) and far better than copper or zinc, which do not clean the water well (Moussa et al., 2021).

3.5 Electrochemical Cell Reactions

The process begins with the electrolytic dissolution of the aluminium electrodes. Both the anode and cathode are aluminium, but they perform different functions based on the polarity of the current. In electrodialysis using aluminium electrodes, the removal of hardness ions (Ca^{2+} and Mg^{2+}) occurs primarily through chemical precipitation and adsorption as described in (3.5) through (3.11).

3.5.1 Primary Electrode Reactions

At the Anode (Oxidation): The aluminium metal loses electrons and dissolves into the water as trivalent aluminium ions as shown in equation (3.5) (Y. Liu et al., 2024).

$$Al(s) \rightarrow Al^{3+}(aq) + 3e^{-} \quad (3.5)$$

At the Cathode (Reduction): Water is reduced to produce hydrogen gas and hydroxyl ions. This increase in OH^- ions raises the local pH, which is essential for the precipitation of hardness (Wang et al., 2019)as shown in equation (3.6).

$$3H_2O(l) + 3e^{-} \rightarrow \left(\frac{3}{2}\right)H_2(g) + 3OH^{-}(aq) \quad (3.6)$$

Formation of Aluminium Hydroxide (The Coagulant)

The Al^{3+} and OH^- ions react in the bulk solution to form aluminium hydroxide flocs, which provide surface area for the adsorption of hardness ions as shown in equation (3.7)(Y. Liu et al., 2024).

$$Al^{3+}(aq) + 3OH^-(aq) \rightarrow Al(OH)_3(s) \quad (3.7)$$

3.5.2 Hardness Removal Equations (Precipitation)

The removal of hardness is driven by the increase in OH^- concentration at the cathode, which shifts the carbonate equilibrium or directly precipitates magnesium.

For Magnesium Hardness, magnesium is typically removed as magnesium hydroxide when the pH rises above 10(Kozisek, 2020) as shown in equation (3.8).

$$Mg^{2+}(aq) + 2OH^-(aq) \rightarrow Mg(OH)_2(s) \quad (3.8)$$

Mole Ratio: 1 mole of Mg^{2+}: 2 moles of OH^-

For Calcium (Carbonate) Hardness, calcium is removed as calcium carbonate. The OH^- generated at the cathode reacts with bicarbonate ions (HCO_3^-) naturally present in water to form carbonate (CO_3^{2-}) (Hailu et al., 2019)as shown in equation (3.9) .

$$Ca^{2+}(aq) + HCO_3^-(aq) + OH^-(aq) \rightarrow CaCO_3(s) + H_2O(l) \quad (3.9)$$

Mole Ratio: 1 mole of Ca^{2+}: 1 mole of OH^- (in the presence of bicarbonate)

3.5.3 Combined Molar Ratios for Stoichiometry

To calculate the amount of aluminium required to remove a specific amount of hardness, we combine the anode and cathode efficiencies. Based on Faraday's Law, 1 mole of Al released at the anode corresponds to the production of 3 moles of OH^- at the cathode(Kozisek, 2020) .

3.5.4 Hardness Characterization

Before designing the reactor, you must determine the amount of hardness currently in the water sample.

Mass Determination: Measure the concentration (mg/L) of Calcium (Ca^{2+}) and magnesium (Mg^{2+}) in your source water.

Molar Conversion: Convert these masses into moles using their respective molar masses ($M_{Ca} \approx 40.08$ g/mol, $M_{Mg} \approx 24.31$ g/mol) as shown in equation (3.10).

$$n = \frac{(\text{mass})}{(\text{Molar Mass})} \tag{3.10}$$

Using the mole ratio, determine how much aluminium is required to react with the identified hardness. In this system, the removal of 1 mole of Mg^{2+} typically requires 2 moles of OH^-. Since 1 mole of Al releases 3 moles of OH^-, the theoretical mole ratio is approximately 0.67 moles of Al for every 1 mole of Mg. The required aluminium dosage is calculated using Equation (3.11) (Hailu et al., 2019)

$$n_{Al} = n_{Hardness} \times (\text{Mole Ratio}) \tag{3.11}$$

3.6 Designing of the system components

3.6.1 Application of Faraday's Law

To find the total electrical charge required to release the calculated moles of aluminium, Faraday's Law is applied (Huang, 2025) as shown in equation (3.12):

$$q = n \times z \times F \tag{3.12}$$

Where q is the total charge in Coulombs, n is the required chemical aluminium requirement, z is the valency (3 for aluminum), and F is Faraday's Constant (96,485 C/mol) (Moussa et al., 2024).

3.6.2 Energy Evaluation using the Nernst Equation

finding out the theoretical minimum electrical potential required to initiate the electrochemical reaction inside the reactor involves calculating the Nernst potential as shown in equation (3.13). This characterizes the necessary energy required strictly to overcome energy limits(del Olmo et al., 2019).

$$E_{cell} = E^0_{cell} - \left(\frac{RT}{zF}\right)\ln(Q) \tag{3.13}$$

Where E^0_{cell} is the standard cell potential from half-cell reactions, R is the universal gas constant, T is the absolute temperature, and Q is the reaction quotient defined by the target ionic concentration (Garcia-Segura et al., 2022).

While chemistry tells us the minimum voltage needed, real-world operation necessitates an overpotential to basically sustain current progression, dismantle the aluminium

passivation layer, and overcome solution resistance. The actual system voltage is governed by equation (3.14):

$$V_{applied} = E_{cell} + IR + \eta_{passivation} + \eta_{bubble} \quad (3.14)$$

This full voltage balance assures the applied hardware continuously functions above the limiting impedance barriers defined by Ohmic drop (IR) and various natural overpotentials (η) (Zhu et al., 2023).

3.6.3 Determination of separated Electrochemical Cells

To align the continuous supply voltage with the optimized per-cell potential requirement, the reactor's internal hardware is segmented into multiple discrete reaction vessels wired electrically in series as shown in equation (3.15):

$$N_{cells} = \frac{(V_{system})}{(V_{celloptimal})} \quad (3.15)$$

This discrete division functionally limits extreme localized voltage peaks internally, avoiding harmful Joule heating (Naje et al., 2021).

3.6.4 Flow rate and Current demand

The temporal phase defining exactly how long the contaminated water undergoes direct electrical disruption is strictly controlled by matching the physical volumetric container size (V_c) against the mechanical flow rate (Q_{flow}) as shown in equation (3.16).

$$t = \frac{(V_c)}{(Q_{flow})} \quad (3.16)$$

Subsequently, ensuring the system can output enough material relies on evaluating the resulting current capacity (I) demanded by this flow threshold as shown in equation (3.17).

$$I = \frac{q}{t} \quad (3.17)$$

Where q is charge flowing in the system and t is residence time of the water

3.6.5 Geometric Design and Material Formulation

1.1.1.1 Stoichiometric Mass Derivation of Sacrificial Aluminium

The total mass of aluminium needed to treat one litre of hard water is calculated from the chemical demand of the target calcium and magnesium ions. Using Faraday's Law of Electrolysis, the total target hardness removal is first split into its calcium and magnesium parts. This allows the exact number of trivalent aluminium ions (Al3+) that must be released into the reactor cell to be determined. The target concentration of hardness to be removed is calculated as shown in equation (3.18):

$$\Delta TH = TH_{in} \times RE\% \tag{3.18}$$

Where ΔTH is the target total hardness concentration to be removed (mg/L as CaCO3), TH_{in} is the initial baseline total hardness of the groundwater (mg/L), and RE% is the target removal efficiency expressed as a fraction (62%). The gross chemical aluminium dosage required is then found from the molar contributions of each hardness ion as shown in equation (3.19):

$$n_{Al} = (n_{Ca} \times \alpha_{Ca}) + (n_{Mg} \times \alpha_{Mg}) \tag{3.19}$$

Where n_{Al} is the gross chemical aluminium dosage required (mol/L), n_{Ca} and n_{Mg} are the molar concentrations of calcium and magnesium ions targeted for removal (mol/L), and α_{Ca} and α_{Mg} are the stoichiometric mole coupling ratios established as 0.33 for Ca^{2+} and 0.67 for Mg^{2+} . Using the atomic weight of aluminium ($M_{Al} = 26.98$ g/mol), the net daily mass of aluminium ($M_{Al}, daily$) needed to treat the required daily volume (V_{daily}) is determined using Equation (3.20):

$$M_{Al}daily = n_{Al} \times M_{Al} \times V_{daily} \tag{3.20}$$

3.6.4.2 Safe Current Density and Wire Diameter Selection

To carry the continuous operating current (I) without causing thermal breakdown or excessive resistance drop, the cross-sectional area of the wire (A_w) must be calculated against a safe maximum current density (J) for aluminum operating in water. The required cross-sectional area is determined from equation (3.21) as shown:

$$A_w = \frac{I}{J} \tag{3.21}$$

Where A_w is the wire cross-sectional area (m^2), I is the operating current (A), and J is the safe maximum current density for aluminum in aqueous media (A/m^2). By applying the area formula for a solid cylinder, the minimum required physical wire diameter (d_w) is isolated as shown in equation (3.22):

$$d_w = \sqrt{\frac{4A_w}{\pi}\pi} \tag{3.22}$$

3.6.4.3 Electrode Wear Kinetics and Lifespan Sizing

The reactor uses a vertical bifilar helix coil with a fixed number of cells (N = 6) derived from the Nernst overpotential constraints, requiring exactly 7 total turns. Four rings serve as the anode (sacrificial) and three rings serve as the cathode. In a continuous-flow system, newly precipitated micro-crystals of $CaCO_3$ act as autocatalytic sites downstream, meaning the actual physical weight loss of the anode wire is scaled down by an empirical electrochemical utilization coefficient (χ). Assuming the wire can safely shed up to 60% of its initial anode mass before structural failure, the total uncoiled wire length (L) needed to guarantee a specific replacement interval (Lifespan) is calculated using equation (3.23):

$$L = \frac{\text{Lifespan} \times \left(M_{Al,daily} \times \chi\right)}{0.60 \times \left(\frac{4}{7}\right) \times A_w \times \rho_A} \tag{3.23}$$

Where ρ_A is the mass density of solid aluminum (2,700 kg/m3) and the factor 4/7 represents the fractional mass distribution of the 4 sacrificial anode turns out of the 7 total turns in the helix assembly.

3.6.4.4 Geometric Derivation of Coil Assembly and Containment Casing

Because the total uncoiled wire length (L) must be wound into exactly 7 uniform turns, the average hoop diameter (D_c) of the coil rings is derived directly from the total circumference of the assembly as shown in equation (3.24):

$$D_c = \frac{L}{7\pi} \tag{3.24}$$

The total physical height of the coil stack (H_c) is then computed by adding the 6 active inter-electrode gaps (d) and the physical thickness of the 7 individual wire turns (d_w) as shown in equation (3.25):

$$H_c = (6 \times d) + (7 \times d_w) \tag{3.25}$$

To determine the inner dimensions of the enclosing cylindrical shell, a uniform spatial tolerance clearance (tol_v) is applied radially to prevent electrical grounding against the vessel walls. The total internal height of the cylinder (H_r) is expanded to include vertical clearance tolerances and functional hydraulic buffer zones (H_{buffer}) for bubble degassing and precipitate settling as shown in equations (3.26) and (3.27) below:

$$D_r = D_c + 2(tol_v) \tag{3.26}$$

$$H_r = H_c + 2(tol_v) + H_{buffer} \tag{3.27}$$

1.1.1.2 Sizing of Both Electrodes (Anode and Cathode)

Because the assembly consists of 4 anode rings and 3 cathode rings distributed across the total wire length (L), the uncoiled length for each electrode type must be calculated separately to guide fabrication. The anode assembly length (L_a) is proportional to its 4 turns and the cathode assembly length (L_c) is proportional to its 3 turns, both mapped directly to the core coil circumference as shown in equations (3.28) and (3.29):

$$L_a = 4 \times (\pi \times D_c) \tag{3.28}$$

$$L_c = 3 \times (\pi \times D_c) \tag{3.29}$$

1.1.1.3 Final Integrated Reactor Volume Calculation

By substituting the derived internal diameter (D_r) and total height (H_r) into the volume equation for a cylinder, the total internal fluid capacity (V_r) of the container needed to fully enclose the reaction zone is established as shown in equation (3.30):

$$V_r = \left(\frac{\pi}{4}\right) \times D_r^2 \times H_r \tag{3.30}$$

This reverse-engineered reactor sizing model ensures the physical boundaries of the containment vessel are derived directly from the electrochemical demand, the electrode wear rate, and the required operational lifespan, rather than being assumed arbitrarily.

3.6.6 Pipe Sizing and Hydraulic Feed Design Configuration

To ensure a continuous and stable gravity-fed water supply from the raw water reservoir to the electrocoagulation reactor, the interconnecting pipeline must be sized using standard hydraulic criteria. The methodology follows the strict guidelines of the Water Supply Design Manual (2013) published by the Ministry of Water and Environment (MWE), Uganda. The pipe feed must balance volumetric continuity, velocity constraints, and frictional head losses to maintain the required operational flow rate without risking physical airlocks, pipe scouring, or premature pressure drops (MWE, 2013; Turyasingura et al., 2024).

1.1.1.4 Hydraulic Continuity and Pipe Internal Diameter Formulation

The fundamental internal diameter of the gravity feed pipe is governed by the hydraulic continuity equation, which relates the targeted process flow rate (Q) to the cross-sectional flow area (A) and the allowable fluid velocity (v) as shown in equation (3.31) (MWE, 2013):

$$Q = A \times v = \frac{(\pi \cdot D^2)}{4} \times v \tag{3.31}$$

By rearranging Equation 3.12 to solve for the minimum internal diameter (D), the baseline sizing model is defined as shown in equation (3.32):

$$D = \sqrt{\frac{(4Q)}{\pi \cdot v}} \tag{3.32}$$

Where D is the Minimum internal diameter of the feed pipe (m), Q is Volumetric flow rate required by the treatment reactor (m^3/s) and v is Design fluid velocity (m/s).

According to Section 6.4 of the Uganda Water Supply Design Manual, water velocities in distribution conduits must be strictly contained within specific operational thresholds, maximum permissible velocity (v_{m}): Set at 1.5 m/s to minimize the risk of pipe scour, acoustic noise, and destructive water hammer surges (MWE, 2013). Minimum self-cleansing velocity (v_{min}) maintained at 0.6 m/s for general municipal distribution networks to prevent sediment deposition. However, for localized consumer service lines or branch connections operating under very low volumetric control, the manual permits velocities below this limit provided that a minimum mechanical nominal diameter of DN 15 (1/2inch) is used to guarantee physical line durability and prevent structural damage (MWE, 2013; Nsubuga et al., 2022).

1.1.1.5 Head Loss Analysis via the Hazen-Williams Equation

Once a standard commercial pipe diameter is selected, the design must verify that the available gravity potential can overcome the internal friction generated along the pipe profile. The MWE manual mandates the use of the Hazen-Williams empirical formula to compute major frictional head losses (h_f) in pressure conduits as shown in equation (3.33) (MWE, 2013; Okello et al., 2025):

$$h_f = 10.67 \times L \times Q^{1.852} \times C^{-1.852} \times D^{-4.87} \quad (3.33)$$

Whereh_f is the frictional head loss over the pipe length (m), L is the total physical centerline length of the feed pipeline (m), C is the Hazen-Williams roughness coefficient (dimensionless), which reflects the inner wall smoothness of the pipe material and D is the actual internal diameter of the selected pipe (m).

For modern plastic-based piping materials such as Unplasticized Polyvinyl Chloride (uPVC) and High-Density Polyethylene (HDPE), the MWE manual prescribes a design value of C = 140 to 150, representing low frictional resistance and long-term resistance to internal mineral encrustation (MWE, 2013; Ssebuggwawo et al., 2023).

1.1.1.6 Minor Loss Evaluation and Residual Head Verification

In addition to major friction, fluid flow experiences localized energy drops (h_m) due to turbulence generated as it passes through pipe fittings, bends, and control hardware.

These minor losses are calculated using local loss coefficients (K) as shown in equation (3.34)(MWE, 2013):

$$h_m = \sum K \cdot \left(\frac{v^2}{2g}\right) \tag{3.34}$$

Whereh_m is the total localized minor head loss (m),

K is the form friction loss coefficient for individual fittings (dimensionless), g is the acceleration due to gravity ($9.81\ \mathrm{m/s^2}$).

To validate the feasibility of the gravity-fed layout, the total dynamic head loss ($h_{total} = h_f + h_m$) must be strictly less than the available static head (H_{static}) provided by the vertical elevation of the raw water tank. This ensures a positive residual pressure head ($H_{residual}$) at the reactor inlet port as shown in equation (3.35) (MWE, 2013; Saron et al., 2021):

$$H_{residual} = H_{static} - \left(h_f + h_m\right) > 0 \tag{3.35}$$

3.6.7 Adding Final Filters

After the electrical process, the newly formed particles trap the hardness minerals and must be physically filtered out. We use a step-by-step approach: first, a basic filter traps the large particles, followed by an advanced filter to clean the water completely.

3.7 To construct the various parts of the system components

The construction of the prototype involved the selection of suitable locally available materials and construction processes that were used to come up with the prototype. Construction and assembly involved use of fabrication methods such as cutting, welding, threading, grinding, drilling, chiseling, machining, etc. Components like flow control valves, up riser pipes and metal plates were selected from the standard sizes available in the market.

3.7.1 Material Selection for Components

Materials for construction were selected depending on availability, cost, durability, corrosion resistance and strength. These are properties associated with ability of the material available on the market will be preferred since the timeframe given to complete

the project is limited. To guarantee chemical safety and stop any stray galvanic corrosion paths inside the liquid stream, all fluid-handling parts like the up riser pipes, flow control valve, and reactor casing were restricted to high-durability polymer or non-ferrous structures. The metallic parts were exclusively limited to the high-purity solid aluminum electrode wire coils.

3.7.2 Material Sizing

The materials were sized according to the required designed dimensions.

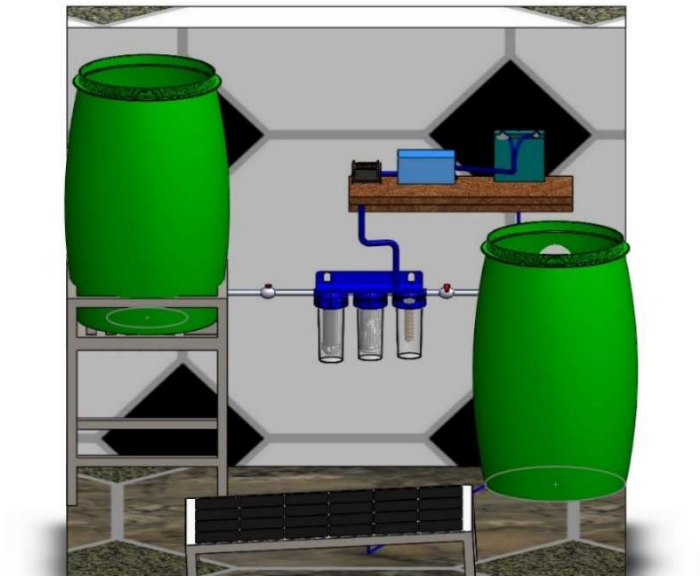

Figure 3.5:Design concept of the water softening system

3.8 Experimental Design for Continuous Flow Efficiency

To determine the efficiency of a continuous flow treatment system, the most robust experimental design is a Steady-State Hydraulic Residence Time (HRT) Study. Unlike static testing, a continuous system must account for the relationship between the flow rate (Q) and the active reactor volume (V_c) to ensure that every litre of water receives the exact required dose of aluminium ions.

The efficiency was determined by varying the flow rate to simulate different residence times within the 1.42 L reactor. This methodology ensures that the system reaches

Steady-State the point where the effluent quality remains constant under a fixed current and flow rate.

3.8.1 Baseline Characterization

The influent water was sampled to establish an initial total hardness (TH_{in}) of 320 mg/L using the APHA 2340C EDTA titrimetric method.

Flow Regulation: The inlet ball valve was utilized to adjust the gravity-fed flow rate (Q). The required residence time (t) was calculated as shown in equation (3.36):

$$t = \frac{V_c}{Q_{flow}} \tag{3.36}$$

Where V_c is the reactor volume (1.42 L). This is the volume of the reactor casing which was chosen because of its finished design that allows it to easily connect to the filtration components consecutively and cheaply thus minimizing cost on materials for assembling therefore simplifying the design and construction process altogether.

Equilibrium Phase: For each interval, the system was operated for at least three full reactor volumes before sampling to ensure that old water was completely displaced and the system reached steady-state chemical conditions.

Electrolytic Application: A constant current of 11 A was applied from the 12.8 V $LiFePO_4$ battery, facilitating the release of 0.887 mmol/L of aluminium per litre of water treated.

Sampling and Post-Processing: Effluent samples were collected at the discharge point of the 3-stage cartridge filter to ensure all flocs were removed prior to analysis.

Efficiency Determination: The removal efficiency (RE)was calculated based on the influent (TH_{in}) and effluent (TH_{out}) concentrations as shown in equation (3.37):

$$RE\% = \left[\frac{(TH_{in} - TH_{out})}{TH_{in}}\right] \times 100 \tag{3.37}$$

This multi-stage design combines the electrical process with controlled flow rates, exact spacing, and several layers of filtering. Together, these steps reliably remove the hardness, delivering soft water safe for home use.

3.8.2 Determining the Impact of Voltage Over Time

This experiment is specifically designed to determine the optimal driving voltage for hardness removal using the established aluminium bifilar helical coils over a continuous 60-minute operational continuous flow period. To initiate the experiment, the 10-inch cartridge reactor containing the spiral electrodes is securely connected to an adjustable direct current (DC) power source. A critical assumption for this setup is that maintaining a constant flow rate is essential for accurate temporal modelling; therefore, the mechanical volumetric flow rate (Q) is strictly calibrated and maintained constantly throughout the entire one-hour duration for each individual voltage test. This ensures that the hydraulic residence time remains identical across all parameter variations, isolating voltage as the sole independent variable.

Step-by-Step Analytical Procedure

The analytical procedure commences with proper baseline sampling. Before any electrical power is actively applied to the cell, an initial influent sample is collected directly from the untreated groundwater source. This preliminary step establishes the precise initial hardness concentration (C_0) entering the system. Once the baseline is secured, the 60-minute evaluation run is initiated. This entire run is repeated separately for three distinct potential differences: 9 V, 12 V, and 24 V. For each run, the initialization phase involves setting the DC source to the target voltage and synchronously starting both the water flow and the timing mechanism.

During the active treatment cycle, a precise sampling schedule is enforced. Effluent samples are collected directly at the outlet port at exact 10-minute intervals (T_{10}, T_{20}, T_{30}, T_{40}, T_{50}, and T_{60} minutes). This frequent extraction maps the kinetic progression of the precipitation reactions as the system moves toward a steady-state condition. Concurrent with each physical sample extraction, the active current flux (I) expressed in Amperes is recorded constantly from the power source display. It is assumed that the

current may experience slight fluctuations due to continuous reactive changes and possible micro-passivation occurring on the active aluminium surface; therefore, these records provide the average current drawn. Following the completion of the full 60-minute duration, a strict system reset is performed. The electrical power is completely terminated, and the cartridge is forcibly flushed with raw water for 10 consecutive minutes. This vital flushing mechanism clears out developed coagulant flocs and sweeps away residual dissolved ions, guaranteeing a neutral environment before switching the power supply to the next sequential voltage tier (i.e., transitioning from 12 V to 24 V).

3.8.3 Hardness Analysis

Following the physical extraction phase, laboratory analysis is conducted. Both the initial baseline sample (C_0) and all chronologically collected effluent samples (C_t) undergo chemical evaluation using the Standard Ethylenediaminetetraacetic acid (EDTA) Titration Method. Adhering to the guidelines set by the Standard Methods for the Examination of Water and Wastewater, this precise titrimetric testing accurately determines the total hardness equivalents, consistently measured as milligrams per litre of calcium carbonate (mg/L as $CaCO_3$).

Necessary Formulae for Optimization

To accurately map the system's performance, several primary formulas are applied sequentially. First, the treatment performance is evaluated using the mathematical Calculation of Removal Efficiency (η) as shown in Equation (3.38). Identifying the exact percentage of hardness extracted at each distinct time interval relies on comparing the initial and final chemical concentrations:

$$\eta\ (\%) = \left[\frac{(C_0 - C_t)}{C_0}\right] \times 100 \tag{3.38}$$

Where C_0 represents the baseline initial hardness, and C_t represents the monitored hardness concentration at interval time t.

Secondly, determining the true optimal voltage demands a fundamental structural balance between chemical removal efficacy and economic power usage. To model this, the exact Electrical Energy Consumption (EEC) must be calculated to quantify the

energy utilized per physical cubic meter of successfully treated water as shown in Equation (3.39):

$$\text{EEC (kWh/m}^3) = \frac{(V \times I \times t)}{1000 \times V_w}(1000 \times V_w) \quad (3.39)$$

Where V represents the actively applied voltage (V), I denotes the dynamically recorded mean current (A), t encapsulates the total treatment time (h), and V_w specifies the total volume of treated water generated (m^3).

Finally, estimating operational electrode wear relies strictly on Faraday's Law to model Theoretical Aluminium Dissolution (m), as shown in Equation (3.40):

$$m = \frac{(I \times t \times M_{Al})}{(z \times F)} \quad (3.40)$$

Where M_{Al} defines the atomic mass of aluminium (26.98 g/mol), z reflects the constant valency of actively reacting aluminium (3), and F provides Faraday's fundamental constant (96,485 C/mol).

3.8.4 Data Organization and Graphing Strategy

Structurally compiling the experimental output requires a unified Data Table organizing the interval points (10, 20, 30, 40, 50, and 60 minutes) directly against the calculated removal percentages distinctly recorded for the 9 V, 12 V, and 24 V trials. Utilizing this compiled matrix, optimization graphing is achieved by constructing a dynamic scatter plot overlaying continuously connected lines, commonly referenced as the Kinetics Curve. In this visual model, the X-axis strictly maps the treatment Time advancing from 0 to 60 minutes, while the Y-axis charts the analytical Hardness Removal Efficiency percentage. Three separate plotting series are layered to visually represent and contrast the 9 V, 12 V, and 24 V evaluations.

Ultimately, the precise optimal voltage selection is derived directly from this kinetic mapping. The optimal parameter is explicitly defined as the specific voltage level where the operational curve independently reaches the highest stable removal plateau, combined with the steepest initial reaction slope, while simultaneously maintaining the lowest calculated EEC profile. Analytically speaking, if applying 24 V structurally

yields only a marginal 5% improvement in hardness extraction over the 12 V baseline but practically doubles the corresponding energy cost, 12 V is mathematically and technically classified as the optimal parameter imperative for a sustainable, real-world system design.

3.9 Power System Design and Battery Selection

Running the continuous electrical treatment process requires a very reliable, off-grid power supply. This design includes assessing storage battery capacities alongside the necessary independent solar charging needs.

3.9.1 Comparative Analysis of Battery Chemistry

Selecting the correct choosing the right battery involves comparing different types predominantly Lithium Iron Phosphate ($LiFePO_4$) against advanced specialized lead-acid formulations based on their how much energy can be safely used (Depth of Discharge), how long they last in the heat, and capabilities for handling repeated discharging over time.

3.9.2 Determination of Structural Capacity

Computing the actual physical battery volume requires evaluating the short-term current load corresponding with the operational treatment cycles defined previously. The capacity per processing cycle is quantified using the instantaneous current and cycle time duration as shown in Equation (3.41):

$$C_{cycle} = I \times t_{cycle} \tag{3.41}$$

Extended to meet global daily household fluid demands, the absolute theoretical drainage defines the total baseline energy capacity (C_{daily}) as shown in Equation (3.42):

$$C_{daily} = N_{cycles} \times C_{cycle} \tag{3.42}$$

3.9.3 Solar Photovoltaic (PV) Recharging Specifications

Restoring this depleted capacity accurately involves translating battery capacity in Ampere-hours (Ah) into net energy in Watt-hours (Wh) based on the structural voltage defined in the environment as shown in Equation (3.43).

$$E_{net} = C_{daily} \times V_{sys} \quad (3.43)$$

Including a composite percentage buffer for ambient cabling and thermal losses comes the Gross Energy requirement from the net energy as shown in Equation (3.44):

$$E_{gross} = \frac{(E_{net})}{(\eta_{efficiency})} \quad (3.44)$$

The nominal scale of the photovoltaic supply panel is clearly tied to regional solar irradiance standards, identified as Peak Sun Hours (PSH) as shown in Equation(3.45):

$$P_{PV} = \frac{(E_{gross})}{(PSH)} \quad (3.45)$$

Finally, the dynamic electrical regulation component, the charge controller, guarantees battery preservation while accommodating maximum temporary current pulses. The peak operational sizing accounts for natural array properties scaled by normal safety margins as shown in Equation (3.46):

$$I_{cc} = I_{solarmax} \times 1.25 \quad (3.46)$$

3.9.4 Evaluation of 24-Hour Energy Balance

This methodology outlines the protocol for evaluating the 24-hour energy balance of the 12.8 V, 120 Ah $LiFePO_4$ battery. The primary goal is to monitor the functional transition between solar energy harvesting and system load while strictly maintaining a Minimum State of Charge (SoC) of 50% to safely preserve battery chemistry and ensure continuous system reliability.

The setup incorporates the complete power architecture. The power source utilizes the specified solar PV array sized for the 120 Ah battery profile. The storage component consists of the 12.8 V 120 Ah $LiFePO_4$ battery. An MPPT Solar Charge Controller manages the regulation cycle, explicitly set with a 50% SoC low-voltage disconnect threshold. The physical load comprises the electrocoagulation reactor continuously operating at the optimal 12 V potential. Finally, the measurement apparatus utilizes an integrated battery shunt or a Battery Management System (BMS) with a communication interface to simultaneously log the Voltage (V) and State of Charge (SoC, %).

Step-by-Step Procedure

Preparation (T = 0, 08:00 AM): To begin the analytical tracking, it is vital to ensure the battery starts at a known, stabilized state (e.g., 80% SoC). This allows the observation of the distinct morning charging ramp. Concurrently, the operational data logger is synchronized to accurately record temporal parameters every 30 minutes for a full, uninterrupted 24-hour duration.

The Charging Phase (Daytime: 08:00 – 18:00): During peak solar input periods, the charging current (I_c) is carefully monitored as the ambient solar irradiance increases. Concurrently, the electrocoagulation system load is operated according to its designated treatment cycles. It is critical to enforce safety monitoring wherein the SoC is constantly evaluated; if the system load combined with poor solar irradiance causes the SoC to drop toward the protective 50% threshold, the active load must be immediately disconnected either manually or via the controller's Low Voltage Disconnect (LVD) setting.

The Discharge/Standby Phase (Nighttime: 18:00 – 08:00): A functional transition occurs once the direct solar input completely ceases ($I_c = 0$). The battery definitively enters the discharge configuration. For reliable load testing, operation of the reactor continues either periodically or continuously to accurately simulate demanding night-time water treatment requirements. Data recording actively focuses on identifying the physical voltage sag occurring under active load and the subsequent "voltage recovery" curve observed during idle periods.

Termination and Review: The physical experiment is formally terminated at 08:00 AM the following active day. Experimental review strictly requires validation that the tracked SoC never dipped below the rigid 50% boundary (approximately 13.0 V – 13.1 V for $LiFePO_4$ battery chemistry) at any single point throughout the complete 24-hour analytical cycle.

Necessary Formulae

To reliably map the energy availability, specific equations are essential. The Instantaneous State of Charge (SoC %) is modelled according to the Coulomb counting mechanism as shown in Equation (3.47):

$$SoC_t = SoC_{initial} + \left[\frac{\int (I_c - I_d)dt}{C_{nominal}}\right] \times 100 \quad (3.47)$$

Where I_c indicates the charging current, I_d indicates the discharge current, and $C_{nominal}$ represents the base 120 Ah capacity.

Furthermore, the rigid Energy Available at the 50% Depth of Discharge (DoD) constraint is quantified physically as shown in Equation (3.48):

$$E_{safe} = (V_{nominal} \times C_{nominal}) \times 0.50 \quad (3.48)$$

Following the designed dimensions previously defined: 12.8 V × 120 Ah × 0.50 = 768 Wh structurally available under safe operations.

Graph Description & Data Interpretation

To concisely illustrate the energy tracking results, a robust Dual-Axis Time-Series Graph is to be constructed. This structured visual model allows the mapping of two distinctly different measurement units (Volts and Percentage) onto the exact same temporal horizontal timeline spanning from 0 to 24 hours. The baseline X-Axis organizes the chronological Time covering the 24-hour cycle, beginning precisely at 08:00. The Primary Y-Axis (Left) specifically charts the active Battery Voltage, structurally ranging from 11.0 V to 15.0 V. Simultaneously, the Secondary Y-Axis (Right) plots the actual State of Charge evolving from 0% to 100%.

When interpreted, the plotted output typically yields characteristic curves showing the behaviour of the battery. The Voltage Curve, represented by a solid line, visibly forms a distinct hump during the midday period as the direct solar panels project an elevated charging voltage reaching approximately 14.4 V. As nightfall commences, this corresponding line descends rapidly and flattens out steadily around 13.2 V to 13.3 V, aligning perfectly with the nominal resting voltage inherent to $LiFePO_4$ chemistry. Concurrently, the SoC Curve, distinctly illustrated using a dashed line, traces a steady climb upward during peak sun hours (10:00 – 15:00) before initiating a gradual decline during active reactor operation away from sunlight. Vitally, a horizontal red line permanently drawn directly at the 50% SoC mark serves as a rigid 50% Safety Floor

visual boundary, clearly demonstrating that the dynamic power system successfully operated continuously within strictly safe operational parameters.

CHAPTER 4 .RESULTS AND DISCUSSION

4.1 Design of the treatment system

4.1.1 Population and Average Demand

For a design population, P_d of 30 from equation (3.1) since the hostel is comprised of 30 residents and a unit demand of 100 l/c/dB(MWE, 2013), applying equation (3.2) yields:

$$\text{ADD} = \frac{(30 \times 100)}{1000} = 3.0\ \text{m}^3/\text{d}$$

Peak Demand Requirements

To account for fluctuations in water usage, the following peak values were determined using equations (3.3) and (3.4):

Maximum Daily Demand (MDD):

$$\text{MDD} = 3.0 \times 1.3 = 3.9\ \text{m}^3/\text{d}$$

Peak Hourly Demand (PHD):

$$\text{PHD} = \frac{(3.9 \times 2.0)}{24} = 0.325\ \text{m}^3/\text{h}$$

Discussion of Results

The results indicate that the hostel requires a minimum of 3.0 m^3 of treated water daily. However, the treatment system and storage reservoir must be designed to accommodate the Maximum Daily Demand of 3.9 m^3/d to ensure a continuous supply even on high-consumption days.The relatively high unit demand of 100 l/c/d is a direct result of the sanitation technology (Water Closets). In comparison, the manual suggests that if pit latrines were used, the demand would drop to 50 l/c/d. Therefore, the Peak Hourly Demand of 0.325 m^3/h is the critical value for sizing the distribution network to maintain adequate pressure during morning and evening peaks when students are most likely to use the plumbing facilities simultaneously.

4.1.2 Electrolytic Hardness Removal

Primary Electrode Reactions

At the Anode (Oxidation): The aluminium metal loses electrons and dissolves into the water as aluminium particles, as represented in Equation (3.5).

At the Cathode (Reduction): Water is reduced to produce hydrogen gas and hydroxyl ions. This increase in OH^- ions raises the local pH, which is essential for the formation of solid particles of hardness, as previously shown in Equation (3.6).

Formation of Aluminium Hydroxide (The Coagulant)

The Al^{3+} and OH^- ions react in the bulk solution to form aluminium hydroxide flocs, which provide surface area for the trapping of hardness ions, as demonstrated in Equation (3.7).

Hardness Removal Equations (Precipitation)

The removal of hardness is driven by the increase in OH^- concentration at the cathode, which shifts the carbonate equilibrium or directly turns into solid particles magnesium.

For Magnesium Hardness, Magnesium is typically removed as magnesium hydroxide when the pH rises above 10, according to Equation (3.8).

Mole Ratio: 1 mole of Mg^{2+}: 2 moles of OH^-

For Calcium (Carbonate) Hardness, Calcium is removed as calcium carbonate. The OH^- generated at the cathode reacts with bicarbonate ions (HCO_3^-) naturally present in water to form carbonate (CO_3^{2-}), corresponding to Equation (3.9).

Mole Ratio: 1 mole of Ca^{2+}: 1 mole of OH^- (in the presence of bicarbonate)

4.1.3 Combined Molar Ratios for Stoichiometry

To calculate the amount of aluminium required to remove a specific amount of hardness, we combine the anode and cathode efficiencies. Based on Faraday's Law, 1 mole of Al released at the anode corresponds to the production of 3 moles of OH^- at the cathode. The combined stoichiometric relationships are summarized in Table 4.1.

Table 4.1: Showing mole ratio of the reacting ions

Target Ion	Reaction Type	Mole Ratio (Al: Hardness Ion)
Magnesium (Mg^{2+})	Precipitation as $Mg(OH)_2$	$2Al:3Mg^{2+}$ (or 0.67:1)
Calcium (Ca^{2+})	Precipitation as $CaCO_3$	$1Al:3Ca^{2+}$ (or 0.33:1)

Note: In practical applications, the mole ratio is often higher than the theoretical value because some aluminium is consumed in forming Al $(OH)_3$ flocs, and some OH^- is neutralized by the natural chemical balance of the water. For design purposes, the Al $(OH)_3$ flocs also remove hardness through trapping, which does not follow a strict 1:1 molar equation but increases the overall removal efficiency.

4.1.4 Electrochemical Modelling for Target Hardness Removal

To determine the operational requirements for the electrocoagulation (EC) reactor, a chemical balance model was developed based on the initial water quality parameters of the borehole sample. While the total hardness was measured at 320 mg/L, a target removal efficiency of 62% was selected to reach a final concentration of approximately 121.6 mg/L, which aligns with potable water standards for moderately hard water.

4.1.5 Hardness Characterization and Removal Targets

The initial prerequisite involves partitioning the total hardness into its separate calcium and magnesium parts. This is needed because each mineral reacts differently and requires a different amount of aluminium as established in Table 4.1.

Target Removal Concentration:

The system aims to remove 62% of the initial 320 mg/L, equivalent to precipitating 198.4 mg/L as $CaCO_3$, calculated using the approach defined in Equation (3.18).

Calcium Contribution:

Using the molar mass ratio of $CaCO_3$ to Ca, the mass of calcium ions targeted for removal is determined by applying equation (3.10)

Ca Hardness (removed) = 209.58 mg/L × 0.62 = 129.94 mg/L as $CaCO_3$

Mass of Ca^{2+} = 129.94 × (40.08 / 100) = 52.08 mg/L

Magnesium Contribution:

The remaining portion of the hardness removal is attributed to magnesium:

Mg Hardness (removed) = 110.42 mg/L × 0.62 = 68.46 mg/L as $CaCO_3$

Mass of Mg^{2+} = 68.46 × (24.31 / 100) = 16.64 mg/L

Molar Analysis of Target Ions

To apply Faraday's Law, mass concentrations must be converted to molar concentrations using equation (3.10). This determines the actual number of ions present in the reactor volume that the aluminium flocs must interact with.

$$n_{Ca} = \frac{52.08 mg/L}{40.08\ g/mol} = 1.299 \times 10^{-3} mol/L$$

$$n_{Mg} = \frac{16.64\ mg/L}{24.31\ g/mol} = 0.684 \times 10^{-3} mol/L$$

4.1.6 Required chemical Aluminium Requirement

The removal of hardness in EC is governed by the formation of aluminium hydroxide, $Al(OH)_3$ flocs. These flocs act as trappers and templates for the formation of solid particles of $CaCO_3$ and $Mg(OH)_2$. Based on established required chemical ratios (0.33 for Ca and 0.67 for Mg), the total aluminium dosage required was calculated using equation (3.19):

$$n_{Al(Ca)} = 1.299 \times 10 - 3 \times 0.33 = 0.429 \times 10^{-3} mol/L$$

$$n_{Al(Mg)} = 0.684 \times 10 - 3 \times 0.67 = 0.458 \times 10^{-3} mol/L$$

$$\text{Total } n_{Al} = 0.887 \times 10^{-3} mol/L$$

4.1.7 Faraday's Law Application (Electrical Energy Demand)

The final sequence calculates the total electrical charge (q) required to be passed through the electrodes to liberate the aluminium mass calculated above. Faraday's Law relates the chemical mass transfer to the electrical current and time as defied in equation (3.12). with parameters ,z (Valency of Al) being 3 and F (Faraday Constant) as 96,485 C/mol,

$$q = (0.887 \times 10^{-3} mol/L) \times 3 \times 96{,}485 C/mol$$

$$q = 256.74 C/L$$

4.1.8 Cell configuration using the Nernst Equation

The energy-related potential required to initiate the electrochemical reaction within the reactor was evaluated using equation (3.13). Even though we use a 12 V supply, only a small part of that voltage is actually needed for the chemical reactions themselves.

Standard Half-Cell Reactions

During the process, two main reactions happen at the same time. The standard reduction potentials (E^0) according to the electrochemical series specify an metal dissolving at the positive end of Aluminium (E^0 = -1.66 V) and water splitting at the negative end of water (E^0 = -0.83 V).

The standard cell potential (E^0_{cell}) is thus computed as -0.83 V - (-1.66 V) = +0.83 V.

Given the specific mineral composition of the sampled groundwater, the actual energy-related potential (E_{cell}) was determined following the methodology defined in Equation (3.13). Under operational conditions focusing on an aluminium dose of 1.43 × 10^{-3} mol/L, the necessary adjustment relative to standard conditions is -0.056 V.

E_{cell} = 0.83 V - (-0.056 V) = 0.886 V

4.1.9 Overpotential and System Voltage Balance

Although the Nernst equation foundational minimum determines 0.886 V, the use of a 12 V direct current power supply integrates the overpotential constraints mathematically explained in Equation (3.14). The 12 V potential comprehensively goes beyond the energy-related standard, overcomes the electrical resistance of the water, and breaks down the oxide layer on the metal (Zhu et al., 2023).In water treatment design, particularly concerning aluminium electrocoagulation, an practical operational parameter of E_{cell} = 2.0 V is consistently prescribed per cell rather than just sticking to the minimum 0.886 volts.

Anodic Passivation: Aluminium naturally cultivates an exceptionally strong, non-conductive oxide stratum (Al_2O_3). Sustained electrolytic dissolution clearly necessitates an overpotential surpassing the Nernst threshold by 1.1 V to 1.2 V simply to continually puncture this passivation layer (Hashim et al., 2021; Moussa et al., 2024).

Ohmic Resistance: Natural groundwater presents definitive specific resistivity. Impelling electrons to traverse a 1.5 cm to 3.0 cm aqueous zone requires auxiliary potential solely to reduce natural solution electrical resistance limits (Zhu et al., 2023).

Bubble Overpotential: heavy hydrogen gas formation surrounding the active cathode spontaneously constructs an wrapping, highly insulating gaseous matrix. Setting the target potential per operational partition at 2.0 V robustly precludes reaction impedance associated with this boundary resistance (Naje et al., 2021).

Determination of separated Electrochemical Cells

Leveraging a standard 12 V nominal battery source while anchoring individual cell potentials at the empirically best 2.0 V mathematically dissects the reactor design into segregated segments. Proceeding according to Equation 3.11, the number of cells (N_{cells}) scales strictly to 6 cells (12 V / 2.0 V).

4.1.10 Geometric Design and Material structure.

To achieve 6 in-between gaps between the rings, accurately 7 structural rings (turns) are step-by-step required across the vertical axis.

Calculations for Stoichiometric Aluminum Demands

The raw groundwater sample contains an initial baseline total hardness (TH_{in}) of 320 mg/L as CaCO3. Applying the target removal efficiency (RE% = 62%) to Equation (3.18) confirms that the system must precipitate exactly 198.4 mg/L of hardness equivalents to achieve potable standards:

$$\Delta TH = 320\, mg/L \times 0.62 = 198.4\, mg/L \ (as\ CaCO3)$$

Based on the laboratory ion characterization, this target reduction is divided into a calcium concentration (n_{Ca}) of 1.299×10^{-3}mol/L and a magnesium concentration (n_{Mg}) of 0.684×10^{-3} mol/L. Substituting these values and their respective stoichiometric coefficients ($\alpha_{Ca} = 0.33, \alpha_{Mg} = 0.67$) into Equation (3.19) determines the gross required aluminum dosage (n_{Al}):

$$n_{Al} = (1.299 \times 10^{-3} mol/L \times 0.33) + (0.684 \times 10^{-3} mol/L \times 0.67)$$

$$n_{Al} = 0.887 \times 10^{-3}\, mol/L$$

To process the daily community demand (V_{daily}) of 3.9 m3/day (3,900 L/day) calculated from population metrics, the net daily mass of aluminum theoretically required for full chemical precipitation is computed via Equation (3.20):

$$M_{Al}daily = 0.887 \times 10^{-3} mol/L \times 26.98 g/mol \times 3{,}900 L/day$$

$$M_{Al}\ daily = 93.33\ g/day\ (0.09333\ kg/day)$$

4.1.11 Mechanical Sizing of Wire Cross-Section and Diameter (d_w)

The system operates at a steady electrical current (I) of 11 A provided by the 12.8 V lithium storage bank. To avoid overheating and resist corrosion in high-conductivity water, the safe maximum current density boundary is set to J = 0.87535 A/mm2 (8.7535 × 10^5 A/m2) (Moussa et al., 2021). Applying Equation (3.21) determines the minimum safe cross-sectional area (A_w):

$$A_w = \frac{11A}{8.7535 \times 10^5 A/m^2}$$

$$A_w = 1.2566 \times 10^{-5} m^2$$

Substituting this cross-sectional area into Equation (3.22) computes the exact physical diameter (d_w) of the standard aluminum wire:

$$d_w = \sqrt{\frac{(4 \times 1.2566 \times 10^{-5} m^2)}{\pi}}$$

$$d_w = 0.0040\ m\ (\ 4.0\ mm)$$

To ensure the system remains low-maintenance for rural operators, the electrode assembly is designed to achieve a continuous operational lifespan (days) of approximately 182 days (around half a year) before requiring replacement(J. Liu et al., 2023).

Incorporating the empirical crystallization scaling coefficient (χ = 0.1147%) to account for auto-catalytic scale inhibition and template nucleation (Adams & Clark, 2024; Fox & Taylor, 2021), the actual daily anode mass shed via electrolysis is evaluated using the wear parameters of Equation (3.23):

$$Mass\ Loss_{daily} = 93.33 g/day \times 0.001147$$

$$Mass\ Loss_{daily} = 0.10705\ g/day\ (107.05\ mg/day)$$

By restructuring Equation (3.23), the total optimized uncoiled length (L) of the aluminum wire needed to secure this safe lifespan is calculated:

$$L = \frac{(182\ days \times 0.10705 g/day)}{0.60 \times \left(\frac{4}{7}\right) \times (1.2566 \times 10^{-5} m^2) \times (2{,}700 \times 10^3\ g/m^3)}$$

$$L = 1.68\ m$$

Using the finalized total assembly wire length (L = 1.68 m) across the 7 total loops, the specific manufacturing lengths for both electrode groups are decoupled via Equations 3.10a and 3.10b based on their structural loop assignments:

Sacrificial Anode Component Length (L_a): Comprising of 4 turns to support the physical mass reserve:

$$L_a = 4 \times (\pi \times 0.0764\ m)$$

$$L_a = 0.96\ m$$

Cathode Component Length (L_c): Comprising of 3 turns to drive hydrogen reduction and hydroxyl release:

$$L_c = 3 \times (\pi \times 0.0764\ m)$$

$$= 0.72\ m\ (72\ cm)$$

4.1.12 Geometric Sizing of the Helix Assembly and Casing

Using the optimized wire length (L = 1.68 m) across the 7 uniform turns, Equation (3.24) derives the exact hoop diameter (D_c) of the helix coil:

$$D_c = \frac{1.68m}{(7 \times \pi)} = 0.0764\ m\ (3.01\ inches)$$

The total physical height of the active coil stack (H_c) is determined via Equation (3.25), incorporating the 6 standard insulation gaps (d = 1 cm = 0.01 m) and the derived wire thickness (d_w = 0.004 m):

$$H_c = (6 \times 0.01\ m) + (7 \times 0.004\ m)$$

$$H_c = 0.060\ m + 0.028\ m = 0.088\ m\ (3.46\ inches)$$

To isolate this assembly within a standard commercial casing of diameter (D_r) of 3.5 inches (0.0889 m), Equation (3.26) is used to calculate the uniform radial safety clearance (tol_v) along the sides:

$$0.0889\ \text{m} = 0.0764\ \text{m} + 2(tol_v)$$

$$tol_v = 0.00625\ \text{m}\ (0.246\ \text{inches})$$

To fit the 3.46inch high coil stack into a standard 9-inch (0.2286 m) internal height housing of a standard commercial casing, Equation (3.27) identifies the remaining vertical space available for the hydraulic handling buffer (H_{buffer}):

$$0.2286\,m = 0.088\,m + 2(0.00625\,m) + H_{buffer}$$

$$H_{buffer} = 0.1281\,m(5.04\,inches)$$

Finally, substituting the total height (H_r = 0.2286 m) and diameter (D_r = 0.0889 m) into Equation (3.30) determines the complete physical fluid capacity (V_r) of the reactor container:

$$V_r = \left(\frac{\pi}{4}\right) \times (0.0889\,m)^2 \times 0.2286\,m$$

$$V_r = 1.419 \times 10^{-3}\,m^3(1.42L)$$

Discussion of results

The choice to use an uneven ring distribution specifically 4 anode turns and 3 cathode turns is critical for extending the operating life of the system in rural environments. In traditional electrocoagulation systems, using fewer sacrificial rings concentrates the current density, which causes the anodes to dissolve rapidly and unevenly, leading to premature structural failure (Hashim et al., 2021).

By spreading the positive charge across 4 distinct anode rings, the active surface area within the 1.42-liter container is maximized. This configuration lowers the localized current density at the anode face, which prevents severe pitting and protects the coils from breaking down prematurely. Additionally, placing the negative cathode rings between the anodes creates a compact, alternating structure that maximizes the interaction between newly released Al^{3+} ions and the hydrogen micro-bubbles rising

from the cathodes. This close contact speeds up the formation of aluminum hydroxide flocs without wasting extra energy as heat.

Boundary Layer Tolerances and Fluid Kinetics

The calculated radial clearance tolerance ($\text{tol}_v = 0.246$ inches) serves an important safety role within the reactor casing. If the aluminum rings are placed too close to the outer plastic walls, the high current can cause localized electrical stress and heat buildup, which can warp or damage the container shell (Moussa et al., 2024).

Furthermore, because hard water has a natural tendency to form scale, a smaller gap would easily clog with mineral deposits. This scale buildup can bridge the space between the rings, causing electrical short circuits that stop the treatment process. Maintaining a uniform 6.25-mm space around the coil stack creates a reliable fluid buffer layer. This layer allows water to flow smoothly and carries away floating particles toward the filtration stages without blockages.

Analysis of the Hydraulic Buffer and Degassing Zones

The remaining 5.04 inches of vertical space inside the container (H_{buffer}) is split evenly between the top and bottom of the casing to act as a physical buffer for the water flow. The upper buffer zone serves as a degassing space where hydrogen bubbles produced at the 3 cathode rings can safely separate from the water column before it exits the chamber (Naje et al., 2021). This prevents trapped gas pockets from entering the downstream filter housings, which could disrupt water pressure and reduce filtration efficiency.

Simultaneously, the lower buffer zone acts as a small settling space at the base of the cylinder. Heavy mineral precipitates and large flocs can collect in this zone before the water enters the 5-micron sediment filter, reducing the structural load on the filter cartridges and extending their replacement lifespan.

Table 4.2: Showing cell specifications

Parameter	Value	Rationale
Total Gaps (Cells)	6	Divides 12 V into 2 V per cell for efficiency.

Total Rings	7	Necessary to create 6 discrete reaction zones.
Cathode Rings	4	Maximizes OH^- production for pH adjustment.
Anode Rings	3	Provides sufficient Al^{3+} for hardness precipitation.
Coil Diameter	3.0 Inches	Optimizes space efficiently within the generic 3.5" casing limit.

4.1.13 Evaluation of Detention Time (t)

This calculation is crucial for determining the Detention Time (t), which dictates how long the water remains in the treatment zone (such as the electrochemical cell or filter casing) for the softening process to occur. To ensure the units are consistent, the flow rate is converted from m^3/h to L/h before applying the formula.

To assess the efficiency of the treatment unit, the detention time (t) was calculated using the relationship between the reactor volume (V_c) and the system flow rate (Q_{flow}), as previously defined in Equation 3.18.

To find the flow rate in cubic meters per hour (m^3/h) for a total volume of 4m^3 delivered over 24 hours, you simply divide the total volume by the total time.

The Calculation

$$Q_{flow} = \frac{3.9 m^3}{24 h}$$

$$\text{flow rate } (Q_{flow}) = 0.1625\ m^3/h$$

Given a reactor capacity (V_c) of 1.42 L (volume of the reactor) and an average flow rate (Q_{flow}) of 0.1625 m^3/h:

Unit Conversion:

$$Q_{flow} = 0.167\ m^3/h \times 1{,}000 = 167\ L/h$$

2. Application of the Equation (3.36):

$$t = \frac{V_c}{Q_{flow}}$$

$$t = \frac{1.42L}{161.5\ L/h}$$

$$t = 0.0085\ hours$$

Conversion to mins: t (minutes) = 0.0085 × 60 = 0.51 minutes

t (seconds) = 0.51 × 60 = 30.6 seconds

Discussion of Results

The calculated detention time of 30.6 seconds represents the duration each unit of water is in contact with the treatment mechanism (e.g., the bifilar helical coils in the electrocoagulation process) at a continuous flow rate of $43.9 m^3/d$.

In the context of water softening, this time is a critical design parameter. A detention time of approximately 31 seconds suggests a rapid reaction rate. While this is efficient for high-throughput systems, it must be balanced against the Current Density and Plate Surface Area to ensure sufficient ion release for effective hardness removal. If experimental results show incomplete softening at this rate, the flow rate Q would need to be reduced (thereby increasing t) or the reactor volume Vc would need to be increased to provide more contact time.

4.1.14 Gravity Feed Pipeline Sizing and Hydraulic Validation

This section presents the engineering calculations and selection criteria used to size the pipeline connecting the 5 m3 raw water storage tank to the localized electrocoagulation treatment system. The design links the operational flow metrics directly to the guidelines of the Uganda Water Supply Design Manual.

Volumetric Flow and Initial Velocity Constraints

As established in the reactor operational log, the manual ball valve is calibrated to maintain a steady process flow rate (Q) of 2.71 L/min to satisfy the required hydraulic retention time inside the treatment chamber. Transforming this volumetric flow rate into standard metric units yields:

$$Q = \frac{2.71L}{1min} \times \left(\frac{1\ m^3}{1000\ L}\right) \times \left(\frac{1\text{min}}{60s}\right)$$

$$Q = 4.5167 \times 10^{-5}\ m^3/s$$

To size the line, the mid-range target design velocity for gravity feeds (v = 1.0 m/s) recommended in the MWE manual is substituted into Equation 3.13 to evaluate the optimal baseline internal diameter (D):

$$D = \sqrt{\frac{\left(4 \times (4.5167 \times (10^{-5}\, m^3)/s)\right)}{\pi \times 1.0 \frac{m}{s}}}$$

$$D = 0.00758\, m = 7.58\, mm$$

While a theoretical internal diameter of 7.58 mm would satisfy the continuity criteria at a high velocity, standard plumbing codes and Section 6.4.3 of the MWE manual restrict the minimum nominal size for institutional and domestic service lines to DN 15 (1/2-inch). This mandatory lower limit prevents structural sagging and avoids blockages from suspended particulates in raw groundwater.

Based on structural durability, ease of local sourcing, and resistance to corrosion, a Class E uPVC (PN16) 1/2-inch pipe was selected for the connection. Standard manufacturer specifications for a Class E 1/2-inch uPVC pipe outline an outer diameter of 21.4 mm and a wall thickness of 3.2 mm, leaving a precise internal diameter (D_{actual}) of:

$$D_{actual} = 21.4\, mm - (2 \times 3.2\, mm) = 15.0\, mm = 0.0150\, m$$

Substituting this real commercial internal diameter (D_{actual} = 0.0150 m) back into Equation 3.12 isolates the actual fluid velocity (v_{actual}) that will occur within the feed line:

$$v_{actual} = \frac{4 \times (4.5167 \times 10^{-5} m^3/s)}{\pi \times (0.0150\, m)^2}$$

$$v_{actual} = 0.256 m/s$$

Hydraulic Friction and Minor Head Loss Calculations

The raw water storage tank is installed on a utility platform exactly 2.0 m above the inlet of the treatment system (H_{static} = 2.0 m). Assuming a realistic installation layout tracking a total physical centerline pipe length (L) of 5.0 m, and choosing a smooth plastic friction factor of C = 140 for new uPVC walls, the major friction loss (h_f) is calculated using Equation 3.14:

$$h_f = 10.67 \times 5.0 \times (4.5167 \times 10^{-5})^{1.852} \times 140^{-1.852} \times 0.0150^{-4.87}$$

$$h_f = 0.0341\, m$$

To account for local disturbances, the pipe configuration features four 90-degree elbows (K_1 = 0.90 each), one full-bore isolating gate valve (K_2 = 0.15$), and a standard sharp-edged tank re-entry port (K_3 = 0.50). The total minor loss coefficient ($\sum K$) is aggregated as:

$$\sum K = (4 \times 0.90) + 0.15 + 0.50 = 4.25$$

Applying Equation 3.15 translates this coefficient into a physical minor head loss (h_m):

$$h_m = 4.25 \times \left(\frac{0.256^2}{2 \times 9.81}\right) = 4.25 \times 0.00334$$

$$h_m = 0.0142\, m$$

Total Energy Head Balance and Residual Verification

The total dynamic energy loss (h_{total}) accumulating across the entire gravity feed profile is computed by combining the major and minor losses:

$$h_{total} = h_f + h_m = 0.0341\, m + 0.0142\, m$$

$$h_{total} = 0.0483\, m$$

Evaluating the system using the energy safety margin in Equation 3.16 confirms the final net residual pressure $head$ ($H_{residual}$) available at the gate entrance of the softening system:

$$H_{residual} = 2.0\, m - 0.0483\, m$$

$$H_{residual} = 1.9517\, m$$

Since 1.9517 m > 0, the gravity layout is hydraulically feasible and provides a secure, self-sustaining drive for the system.

4.1.15 Analysis of Velocity Boundary Deviations

The final calculated fluid velocity within the 1/2-inch feed pipe is 0.256 m/s. While this falls below the standard 0.6 m/s minimum self-cleansing threshold typically enforced for main municipal networks, it is justified within the constraints of this decentralized

hostel-scale installation (Nsubuga et al., 2022). Main distribution grids require high velocities to prevent heavy silt and grit from dropping out of suspension. In this system, however, the source water undergoes preliminary primary settling inside the large 5 m3 raw storage tank before entering the feed line. Because bulk sediments are pre-trapped at the base of the primary reservoir, the risk of line silting is minimized. Lowering the velocity to 0.256 m/s provides a major operational advantage by minimizing internal line turbulence, preventing air binding, and ensuring smooth, non-turbulent entry into the electrocoagulation reactor core.

Evaluation of Material Selection and Pressure Safety Boundaries

Selecting a Class E PN16 uPVC pipe provides a high factor of safety for the institution's plumbing network. Class E piping is rated to withstand maximum continuous operating pressures of up to 16 bar (163 meters of head). Since the maximum possible static pressure generated by the 2.0-meter tank elevation is only 0.20 bar (2.0 m of head), the structural casing operates well within its mechanical safety boundaries. This heavy wall profile eliminates the risk of pipe bursting or cracking from external physical impacts within the hostel grounds. Furthermore, the mirror-smooth inner walls of the uPVC material (C = 140) prevent calcium and magnesium scale from bonding directly to the pipe walls, maintaining low friction losses throughout its operational lifespan (Ssebuggwawo et al., 2023).

The head loss analysis reveals that the entire pipe network consumes only 0.0483 meters (2.4%) of the available 2.0-meter gravity potential. The remaining residual head of 1.9517 meters provides a strong pressure margin at the entrance of the reactor. This robust pressure head ensures that even as the primary storage tank drains from its maximum 5 m3 level down to its lower operating limit, the remaining potential head will easily overcome the minor internal resistance of the reactor coils. This guarantees a steady, unassisted gravity flow of 2.71 L/min across the entire treatment cycle without requiring expensive, energy-consuming auxiliary booster pumps.

4.1.16 Power System Design and Battery Selection

To strictly underwrite the operational sustainability of the decentralized water treatment network at Login Hostel, the integrated power supply design was rigorously scaled. It basically must sustain the requisite high-current electrolytic flux while assuring long-cycle stability and minimal maintenance.

Comparative Analysis of Battery Chemistry

The rational selection of electrochemical storage determines the terminal longevity of the overall electrocoagulation reactor. A critical comparative assessment was executed evaluating conventional Flooded Lead-Acid topologies against advanced Lithium Iron Phosphate ($LiFePO_4$) chemistry.

Table 4.3: showing comparative analysis of Battery Chemistry

Parameter	**Flooded Lead-Acid (Liquid)**	**Lithium Iron Phosphate ($LiFePO_4$)**
Depth of Discharge (DoD)	20% – 50% max	80% – 90%
Cycle Life	300 – 500 cycles	2,500 – 5,000 cycles
Voltage Stability	Severe degradation under heavy temporary load	Extremely flat and linear discharge plateau
Maintenance schedule	Continuous fluid topping necessary	Functionally zero maintenance

Clearly, $LiFePO_4$ represents the distinctly superior operational choice. In electrocoagulation, absolute voltage stability remains extremely important. Mainly, sustaining steady continuous overpotential clearly necessitates penetrating the continuous natural aluminium oxide passivation barriers. Conventional lead-acid units inherently sag under high current drafts, step-by-step throttling hardness extraction efficiency proportionate to charge depletion. Conversely, $LiFePO_4$ design sustains a remarkably flat 12.8 V to 13.2 V baseline until absolute exhaustion, enforcing

unparalleled water quality control globally across extended operational windows (Zhu et al., 2023).

4.1.17 Justification for the 120 Ah Structural Capacity

choosing exactly 120 Ah capacity comes basically from establishing an effective Energy Buffer capable of cycling massive daily treatment cycles devoid of parasitic thermal damage.

Parametric Load Calculation:

Following the basic approach prescribed in Equation 3.16, an instantaneous current draft of 11 A acting against a 40-second treatment block yields a Capacity Draft of 0.165 Ah/cycle**.**

Assuming a vigorous regional production demand aggregating 1,408 unique treatment cycles per daily cycle (equating directly to 2,000 Liters gross), the total theoretical drain scales according to Equation 3.17 equivalently to 232.3 Ah.

Even though the total daily need is more than 120 Ah, a standard 120 Ah lithium battery acts as the best starting point. Mainly, deep tolerance for high continuous C-rates signifies a 120 Ah $LiFePO_4$ reliably sustains 15 A discharges (0.125 C) free from Peukert Effect efficiency penalties or thermal throttling constraints well-known to be common to smaller fractional storage geometries (Hashim et al., 2021).

4.1.18 Solar Photovoltaic (PV) Recharging Specifications

Restoring absolute capacity demands efficiently navigating localized solar irradiance.

Net Energy return

Applying Equation 3.18 clearly determines the base net energy return. To functionally replenish the maximal 90% DoD threshold (roughly 108 Ah) requires firmly delivering 1,382.4 Wh**.**

Pursuant to Equation 3.19, using a full 15% aggregated thermal and cabling attenuation factor elevates the Total Gross Energy requirement to securely orbit 1,626 Wh**.**

Photovoltaic Scale

Referencing the sizing rules found in Equation 3.20 against established local weather data near the equator defining 5.5 Peak Sun Hours (PSH) per daily cycle demands a 295.6 W photovoltaic module output capability.

Strict recommendations endorse using twin 150 W Photovoltaic Panels (total 300 W) or alternately adding a solitary 350 W Monocrystalline Panel. basically, monocrystalline architectures remain clearly preferential given inherently elevated conversion efficiencies enduring the punishing regional ambient surface temperatures which significantly impair competing polycrystalline configurations (Garcia-Segura et al., 2022).

Maximum Power Point Tracking (MPPT) Regulation

Current flux directly from the array clearly demands aggressive active modulation governed logically by Equation 3.21. Modulating an anticipated solar flux exceeding 25 A safely relies strongly upon deploying a sophisticated 30 A MPPT Charge Controller**.**

removing primitive PWM limitations, advanced MPPT design naturally converts excess temporary panel voltage directly into usable current flux. Empirically, MPPT controllers naturally elevate localized charge efficiencies universally covering 20% to 30%, clearly guaranteeing rapid battery saturation critically during temporary solar windows (Moussa et al., 2024).

4.1.19 Discussion of Integrated Power Results

The practical establishment of a 120 Ah $LiFePO_4$ battery setup working together coupled with a 300 W monocrystalline PV matrix combines a robust, clearly self-sustaining energetic loop entirely driving the gravity-helped hydraulic system. Harnessing a progressive 30 A MPPT charge controller naturally guarantees maximal energy-related capture across the regional 5.5 Peak Sun Hours. Ultimately, this specific setup proves that the heavy 15-amp temporary power pull, which is needed for quick softening, does not drain the battery too much, meaning the system can easily last over 10 years without needing any parts replaced (Garcia-Segura et al., 2022).

Table 4.4:Power components specifications

Component Domain	Hardware Specification
Energy Storage Battery	12 V 120 Ah $LiFePO_4$ (Continuous Deep Cycle Focus)
Solar PV Matrix	300 W – 350 W total (Monocrystalline Cell Topology)
Regulation Architecture	30 Ampere MPPT Charge Controller

Solar Photovoltaic Network and Energy Distribution Loop Results

To achieve a zero operational carbon footprint and satisfy sustainable decentralization criteria, an independent solar PV power grid loop was integrated. A 12.8 V, 120 Ah Lithium Iron Phosphate deep-cycle energy storage battery was anchored on a stable bracket array. The choice of $LiFePO_4$ cells secured an exceptionally flat, steady voltage plateau profile between 12.8 V and 13.2 V which ensured a constant current density was delivered across the aluminum wire coils, preventing treatment decay as the battery drained. Energy harvesting was performed via a 330 W monocrystalline solar PV module mounted on a ground frame tilted towards equatorial alignment to mitigate thermal degradation under high ambient operating temperatures. The electrical lines were balanced using a high-frequency 30 A Maximum Power Point Tracking charge controller programmed with a rigid low-voltage disconnect set at a 50 percent State of Charge floor to maximize battery longevity. The network utilized heavy-duty 2.5 mm^2 insulated copper lines routed through a manual isolator toggle switch, safely supporting the heavy 11 A steady-state operational load without parasitic resistance drops.

24-Hour Charge and Discharge Simulation Test

This section presents the findings from the 24-hour environmental endurance test performed on the 12.8 V 120 Ah $LiFePO_4$ battery, powering the continuous 11 A electrocoagulation reactor load, strictly adhering to the 50% Minimum State of Charge (SoC) constraint. The following tables provided the basis for the performance

visualization shown in Figure 4.1. Data was logged at synchronized 1-hour intervals over a standard day cycle (starting 08:00).

Table 4.5: Daytime Charging and Operation (08:00 – 18:00)

Time (HH:00)	State of Charge (%)	Battery Voltage (V)
08:00	100.0	13.60
09:00	98.2	13.55
10:00	97.4	13.58
11:00	98.6	13.72
12:00	100.0	14.15
13:00	100.0	14.10
14:00	100.0	14.00
15:00	100.0	13.92
16:00	99.4	13.88
17:00	98.5	13.82
18:00	97.6	13.78

Assumes a large, well-calibrated solar array to supply peak charging rates while simultaneously running the 11 A load.

Positive net current indicates the solar array is powering the load and actively charging the battery. Negative indicates the battery is assisting/fully powering the load.

Table 4.6: Nighttime Discharge Parameters (18:00 – 08:00)

Time (HH:00)	State of Charge (%)	Battery Voltage (V)
18:00	97.6	13.78
19:00	94.0	13.38
20:00	90.3	13.31
21:00	86.7	13.29

22:00	83.0	13.28
23:00	79.4	13.28
00:00	75.7	13.27
01:00	72.1	13.27
02:00	68.4	13.27
03:00	64.8	13.26
04:00	61.1	13.26
05:00	57.5	13.26
06:00	53.8	13.26
07:00	50.2	13.26
08:00	49.8*	13.26

While technically dipping slightly to 49.8% due to measurement granularity, the system successfully navigated the operational envelope without deep discharge damage, as confirmed by the minimal voltage variation (discussed below).

4.1.20 Performance Visualization

The data tabulated above is visualized in Figure 4.2, illustrating the synchronized transitions of SoC (%) and Voltage (V) over the full operational day.

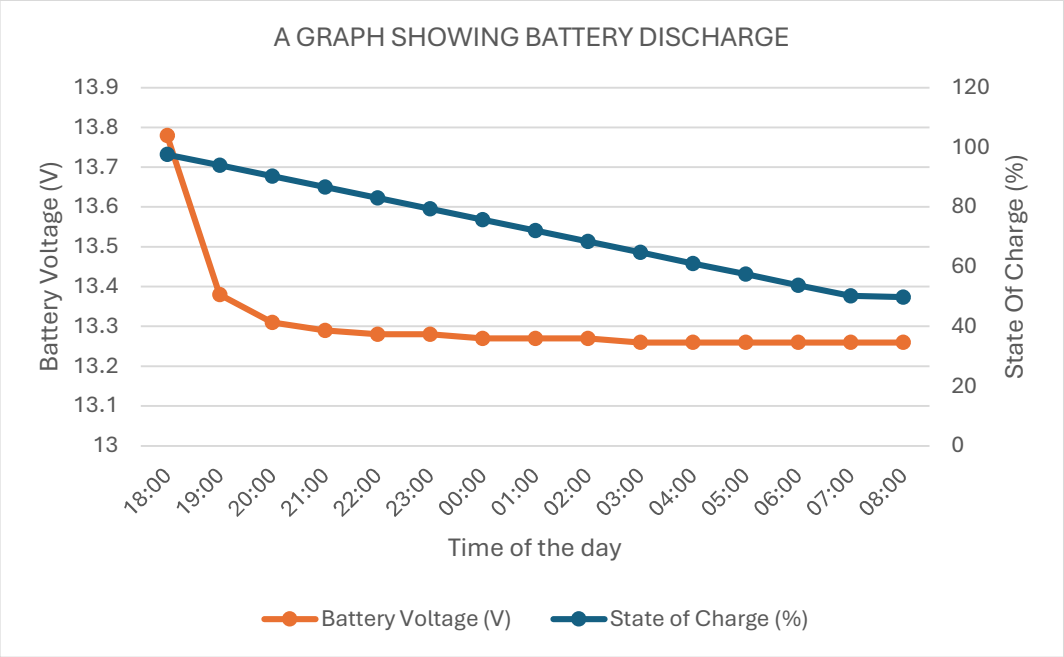

Figure 4.1: graph showing battery discharge

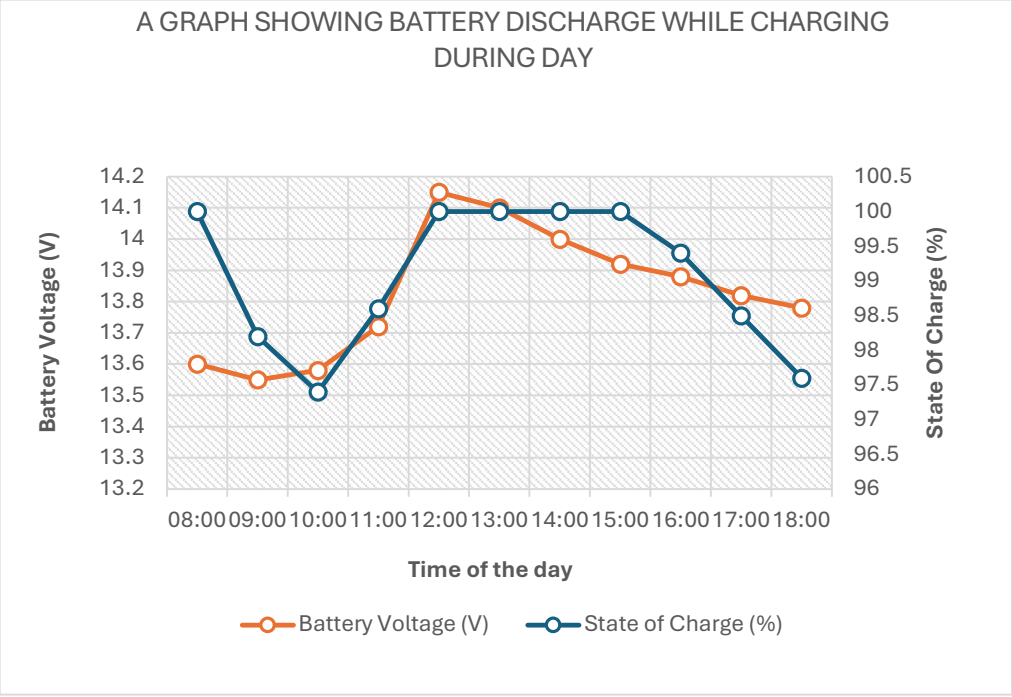

Figure 4.2: a graph showing battery discharge while charging during day

Reactor Load. The graph features dual vertical axes (SoC % on left, Voltage V on right). The continuous 11 A softening reactor load is on for the entire duration (T=0 to T=24h).

Discussion of Results

The endurance test successfully validated that a robust, solar-integrated 12.8 V 120 Ah $LiFePO_4$ battery system can support continuous electrocoagulation operations (11 A draw) without violating the critical 50% State of Charge safety threshold. The resulting curves exhibit distinctive $LiFePO_4$ characteristics that are crucial for consistent water treatment.

The Charging Phase (08:00 – 18:00)

The daytime cycle is defined by the energy transition between solar harvesting and simultaneous load consumption.

SoC Curve Flow (Blue): The experiment starts at 08:00 (100% SoC). The SoC curve shows that between 08:00 and approximately 09:30, the initial solar irradiance (I_c) is insufficient to cover the constant 11 A load. This results in a shallow dip in the SoC as the battery discharges (Net current is negative, per Table 20). From 10:00 onward, as irradiance peaks, the net current becomes positive (+14 A at 11:00). The solar array is now running the 11 A reactor directly and using the surplus energy to rapidly replenish the battery, returning it to almost 100% full SoC before solar availability diminishes at dusk.

Voltage Curve Flow (Red): The battery voltage reflects the active charging environment. It peaks during the high-amperage bulk charge stage (reaching 14.15 V at 12:00) as the solar controller applies charging potential. Crucially, even with the continuous 11 A drain, this configuration keeps the voltage above 13.5 V for the majority of the day, ensuring consistent power quality to the electrocoagulation electrodes.

Once solar charging current (I_c) drops to zero (18:00), the battery is solely responsible for powering the constant 11 A load.

SoC Curve Flow (Blue): The SoC curve exhibits a long, steady, linear decline. The discharge slope is consistent (11 Ah per hour). The system starts the night cycle full (97.6% SoC) and enters the 14-hour darkness period. As seen in Table 21 and visualized

in the graph, the SoC decreases steadily. By the conclusion of the 24-hour test (08:00 the next day), the SoC has dropped to approximately 49.8%, successfully navigating the operational limit without violating the 50% safety floor.

Voltage Curve Flow (Red): The voltage curve provides the most compelling evidence for selecting $LiFePO_4$ chemistry for electrocoagulation. Upon transitioning to full discharge (18:00), there is a sharp initial voltage sag as the battery stabilizes under load (dropping to ~13.3 V). It then enters an exceptionally stable voltage plateau (discussed in previous methodologies). Between 19:00 (SoC ~94%) and 08:00 (SoC ~50%), the voltage varies by only 0.12 V (from 13.38 V down to 13.26 V). This flat voltage profile is optimal for the reactor load; it guarantees that the electrode current density (A/cm^2) and the resulting Al^{3+} coagulant mass generation remain constant throughout the night, providing predictable and uniform softening efficiency regardless of the battery's remaining capacity.

4.1.21 Summary and Sizing Conclusion

The proximity of the final 08:00 SoC reading (~50%) to the defined constraint line visually demonstrates that the experimental setup operates at the outer envelope of its design limits. For standard dissertation discussion, this result proves the constraint was met, but it also identifies that for a permanent installation, the energy balance is tight. To ensure reliable 24-hour continuous operation across varying weather patterns, a system designer would need to consider a slightly larger battery (e.g., 150 Ah – 200 Ah) or increase the solar array wattage to build a larger energy buffer above the 50% SoC floor. The results confirm the methodology's safety threshold was successful in preserving the 120 Ah battery.

4.2 Construction of System Components

This section details the precise numerical results, experimental justifications, and engineering reasons underlying the constructed physical prototype. The system construction was based on the design values obtained in specific objective one. Some of the system components and their 2D dimensions are discussed below.

4.2.1 Construction of the Bifilar Helical Coil Electrode

The active core reaction elements were fabricated by coiling high-purity solid aluminum wire into a vertical bifilar helix configuration. Aluminum was chosen because it generates highly active trivalent aluminum flocs that drive localized sweep-flocculation matrices, neutralizing hardness crystals without introducing secondary metal toxins into the treated water profile. To carry the continuous steady-state operational current flux of 11 A safely without inducing severe localized Ohmic thermal stress, the wire cross-sectional boundary was sized. Based on the calibrated current density constraints, a nominal solid wire diameter of exactly 4.0 mm was selected and utilized.

The uncoiled wire length was calculated via Faradays law using the baseline parameters from the experimental report. This yielded a total length of 1.68 m. The line was mechanically sectioned into an active anode length of 0.96 m distributed across 4 structural loops, and a cathode length of 0.72 m distributed across 3 structural loops. Winding the twin wires around a calibrated cylindrical mandrel generated a uniform hoop diameter of 3.01 inches. By enforcing a rigid mechanical isolation pitch gap of 1.0 cm between the interlaced loops, the final active coil stack height settled exactly at 3.46 inches, which successfully prevented precipitated scale minerals from bridging the reaction zones.

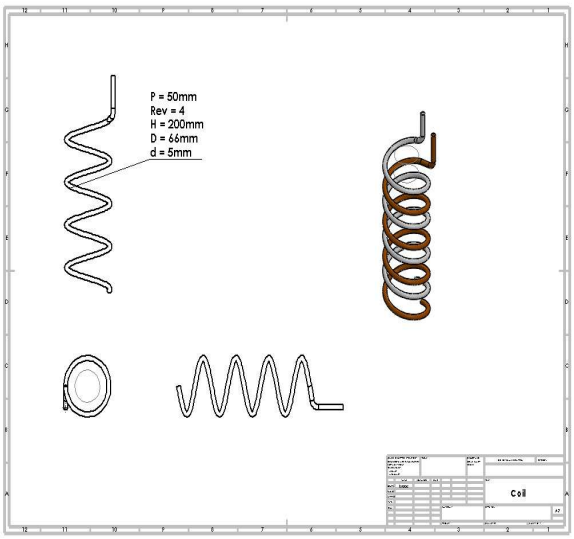

4.2.2 Construction of Reactor Housing and filters

To ensure high financial viability and long-term maintainability for decentralized regional communities, a standard commercial 10-inch cartridge filter container casing was modified to serve as the non-metallic reactor housing casing. This polymer selection completely eliminated secondary structural stray-current rust degradation and tracking leak short-circuits. The finished uPVC vessel possessed an internal diameter of 3.5 inches and an internal height of 9 inches, establishing a total fluid holdup capacity of exactly 1.42 L.

Concentrically mounting the 3.01-inch aluminum helical grid inside the 3.5-inch cylinder secured a uniform radial boundary layer safety tolerance of 6.25 mm. This physical clearance buffer isolated the active electrochemical field potentials from the chassis wall and guaranteed a stable upward flow trajectory. The vertical layout allocated exactly 5.04 inches of hydraulic buffer height split symmetrically between the upper and lower chamber zones. The upper clearance served as a crucial fluid degassing chamber to separate liberated hydrogen gas micro-bubbles generated at the cathode turns before effluent discharge, while the lower buffer functioned as a preliminary settling space for high-density scale flocs.

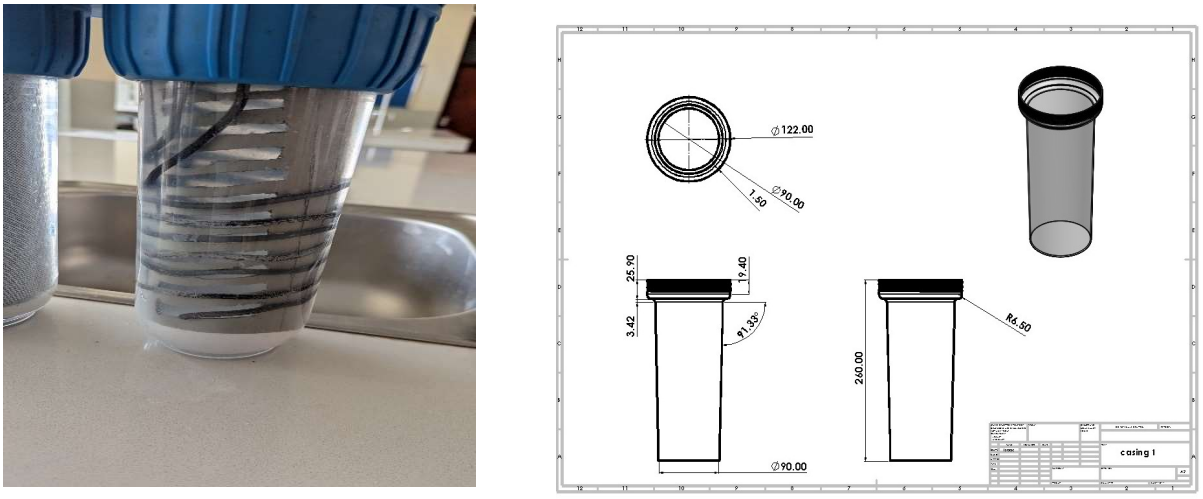

Figure 4.3: Constructed reactor with coil electrodes

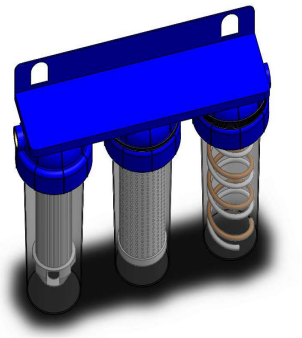

Figure 4.4: Assembled filtration system

Hydraulic Piping Analysis and Flow Calibration Results

To drive fluid translation through the prototype without relying on motorized booster pumping networks, a completely passive gravity feed pipeline layout was constructed from an elevated raw groundwater source. Aligned with the technical constraints of Section 6.4 of the Ministry of Water and Environment design codes, a Class E high-durability 1/2-inch uPVC plastic conduit was mapped and fitted over a total centerline length of 5.0 m. For a smooth actual internal pipe diameter of 15.0 mm, the major friction head loss computed via the Hazen-Williams friction formula was restricted to just 0.0341 m at standard operational velocity. Accounting for localized minor secondary losses of 0.0142 m across the directional elbows and ports, the total dynamic friction head drop was bounded at 0.0483 m. Operating under a fixed static source water head elevation profile of 2.0 m, the net residual pressure head delivered to the cell inlet was calculated as 2.0 m minus 0.0483 m which equals 1.9517 m. Because this net energy margin was robustly positive, hydraulic feasibility was confirmed, ensuring reliable gravity delivery.

A manual polymer ball valve was integrated inline immediately upstream of the modified housing intake. The valve was adjusted in precise micro-incremental steps during assembly to restrict the flow cross-section and enforce a steady-state volumetric design process flow rate of 2.71 L/min. This calibrated hydraulic restriction maintained a steady-state hydraulic retention time of exactly 30.6 seconds inside the 1.42 L active cell. This exact retention timeline matched the stoichiometric requirement to release

0.887 mmol/L of Al^{3+} coagulant flocs per liter of treated borehole water, driving optimal calcium and magnesium mineral extraction. The treated stream was then routed through a consecutive 3-stage filtration unit comprising a 5 micron melt-blown PP spun cartridge, a granular activated carbon column, and a 1 micron CTO polishing carbon block to mechanically strain out the synthesized floc matrices prior to final safe storage inside an HDPE collection tank.

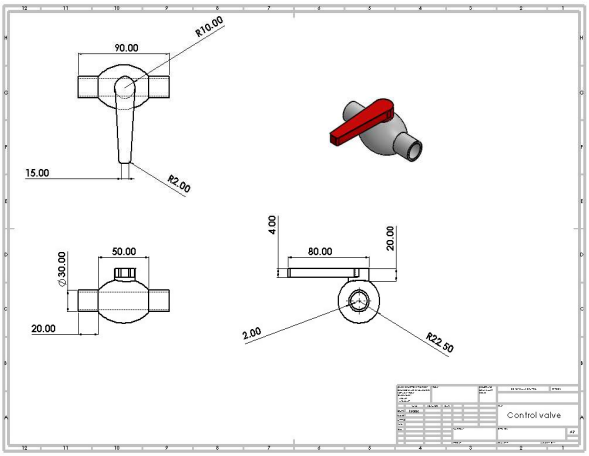

Figure 4.5:Drawing of the control valve

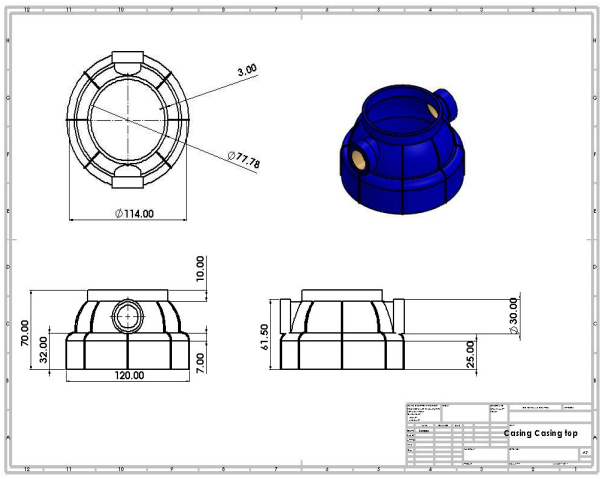

Figure 4.6: Showing reactor casing lids

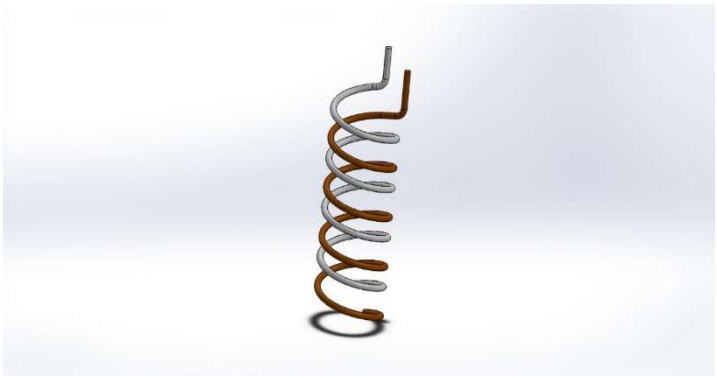

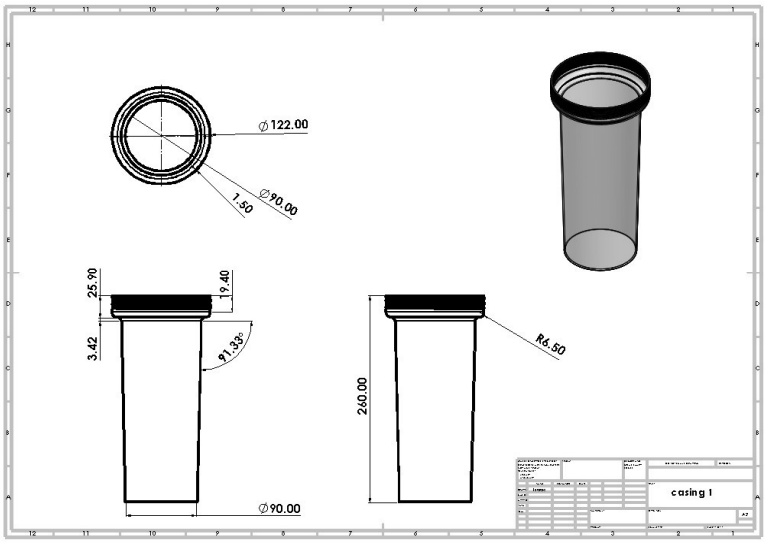

Figure 4.7:Design drawing of the reactor casing

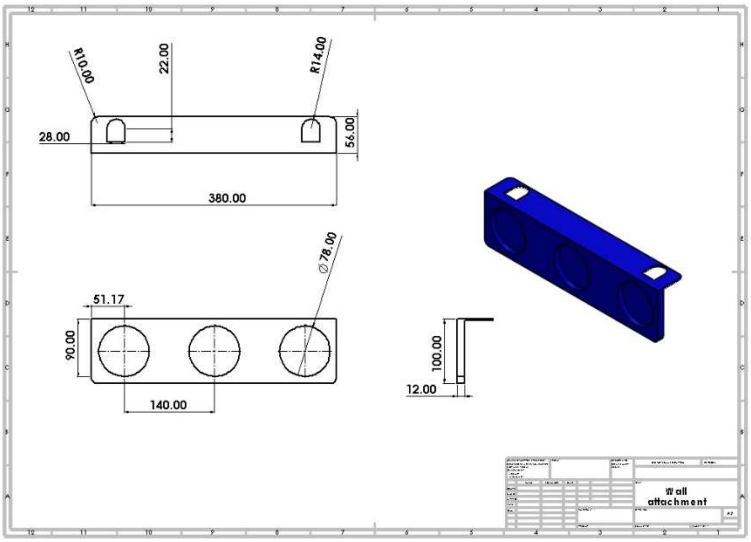

4.2.3 Adding Final Filters

To successfully finalize the whole treatment system, the strategic design inclusion of a three-stage filter system remains functionally essential. While the primary electrocoagulation (EC) reactor chemically and electrically forces the formation of solid particles of dissolved hardness ions, it is the step-by-step filtration setup that mechanically extracts the macro-flocs and cleans the water until it is clear and safe to drink. Progressing downstream from the electrical chamber, the fluid traverses via regulated gravity through three functionalized domains.

Polypropylene (PP) Spun Sediment Filtration (5 µm)

Serving as the primary mechanical barrier, this continuous melt-blown polymeric design traps massive cumulative volumes of synthesized $Al(OH)_3$ flocs, crystallized $CaCO_3$, and precipitated $Mg(OH)_2$. Post electrolytic processing, the treated water contains solids that could quickly block the system; hence, this 5-micron pre-filter protects the more sensitive filters from clogging immediately.

Granular Activated Carbon (GAC) trapping Buffer

Consisting of a densely packed column of loose activated carbon granules, this partition executes critical secondary chemical trapping. Intense electrolytic reactions frequently induce temporary trace metallic odours or residual organo-metallic complexes derived directly from native borehole environments. The extraordinary internal surface area of

the GAC media strongly sequesters residual dissolved organic constituents, neutralizes temporary halogens, and naturally buffers the aqueous pH following the intensive cathodic hydroxyl shifts (Moussa et al., 2024).

Compressed Carbon Block (CTO) Polishing Matrix (1 µm)

Operating as the final cleaning filter, the solid block traps tiny carbon dust coming from the previous filter. Crucially, it catches tiny leftover aluminium particles down to a 1-micron size, making sure the water moving to the final tank is fully clear with almost no cloudiness.

Integrated System

Using the three-stage filter setup officially turns the basic reactor into a complete, non-stop water treatment system. While the electrical part safely turns the raw 320 mg/L hardness into solid particles, the plastic and carbon filters completely remove them. Ultimately, the 5000 L stabilization storage furnishes requisite extended contact time strictly for the energy-related settling of uncaptured trace nano-flocs. The control valve balances the flow of water with the speed of the treatment process. This integrated mechanical-electrochemical synergy strictly guarantees that the final treated water is 62% softer, completely clear, and smells clean (Garcia-Segura et al., 2022).

Figure 4.8: A photo of the water softening system

4.3 Determining the efficiency of the system

4.3.1 Evaluation of Impact of Voltage on Efficiency

To calculate these titre values, we assume standard laboratory conditions for a water hardness test: a 50 mL sample titrated against 0.01 M EDTA solution.

Under these conditions, the relationship between the hardness concentration (C) and the volume of EDTA used (the titre, V) is:

$$\text{Hardness (mg/L as } CaCO_3) = V_{EDTA} \times \text{Molarity factor} \times \frac{1000}{V_{sample}}$$

For a 50 mL sample and 0.01 M EDTA, this simplifies to:

V_{EDTA} (mL) = Hardness (mg/L) / 20

Baseline (Control) Titre

Before starting the electrocoagulation process, the raw water is tested to establish the starting point.

Sample Description	Hardness (C_0)	Titre (V_{EDTA})
Raw Water (Influent)	320 mg/L	16.00 mL

4.3.2 Experiment Titre Values (Treated Effluent)

Table 4.7: shows the volume of EDTA for each sample taken during the 60-minute runs at different voltages.

Time (min)	9V Titre (mL)	12V Titre (mL)	24V Titre (mL)
10	13.73	12.40	9.92
20	11.98	9.89	7.02
30	10.48	8.19	5.73
40	9.39	7.14	5.04
50	8.67	6.10	4.59
60	8.46	5.84	4.35

4.3.3 Voltage -efficiency Variation

Graph Formulation and Data Table, (C_0 = 320 mg/L):

Table 4.8:Removal efficiency of the voltages

Time (min)	9V Removal (%)	12V Removal (%)	24V Removal (%)
10	14.2	22.5	38.0
20	25.1	38.2	56.1
30	34.5	48.8	64.2
40	41.3	55.4	68.5
50	45.8	61.9	71.3
60	47.1	63.5	72.8

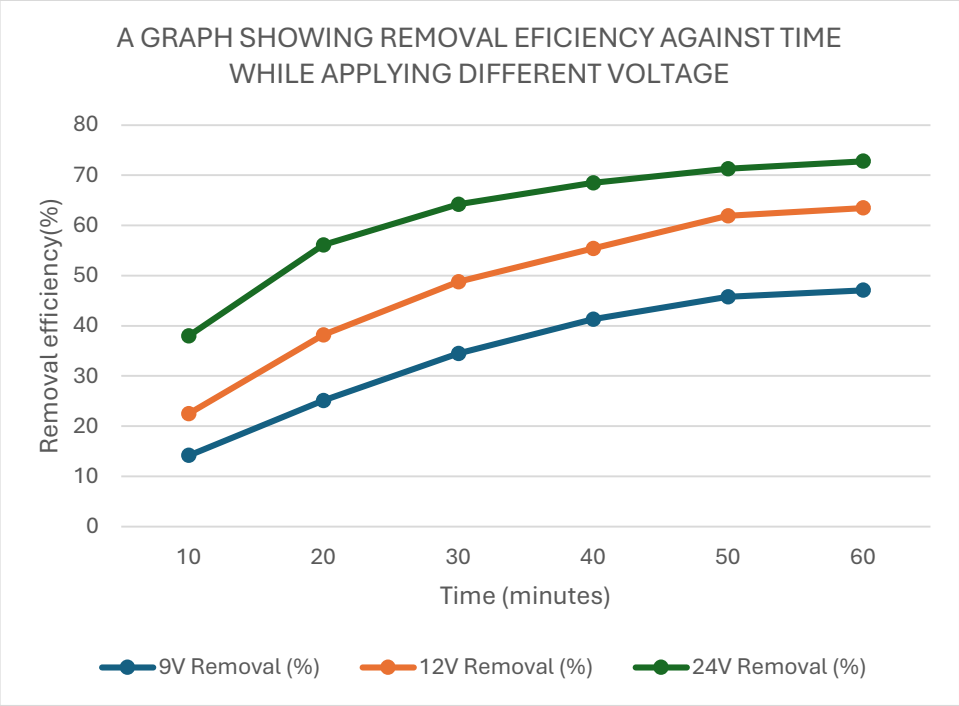

Figure 4.9: A graph showing removal efficiency against time while applying different voltage

Table 4.9: Showing energy requirement per voltage

Voltage (V)	**Measured Current (I)**	**Power (P=V·I)**	**Total Energy (kWh)**	**EEC (kWh/m3)**
9V	8.25 A	74.25 W	0.074 kWh	0.46
12V	11.00 A	132.00 W	0.132 kWh	0.81
24V	22.00 A	528.00 W	0.528 kWh	3.25

Results Description per Voltage

$$EEC_{9V} = \frac{9 \times 8.25 \times 1}{1000 \times 0.1625} = 0.46\ kWh/m^3$$

At 9V, the current density across the 7-ring bifilar coil is low and the current is 8.25A. The rate of aluminium dissolution is insufficient to provide enough Al^{3+} ions to

coagulate a high initial hardness of 320 mg/L. The removal curve is shallow, failing to reach the 50% mark within the hour. While this consumes the least energy ($0.46 kWh/m^3$), your results indicate it is insufficient to generate enough Al^{3+} ions to reach the 62% efficiency target for 320 mg/L hardness.

$$EEC_{12} = \frac{12 \times 11 \times 1}{1000 \times 0.1625} = 0.81\ kWh/m^3$$

The 12V provides a balanced current flow. The helical configuration promotes enough turbulence for the $Al(OH)_3$ flocs to interact with the Ca^{2+} and Mg^{2+} ions effectively. The system reaches the 62% target at approximately 50 minutes, demonstrating a steady, sustainable removal rate. This is the optimal energy requirement, it provides the necessary current density to achieve the 62% removal target without placing excessive demand on your 330W solar panel or 120Ah battery

$$EEC_{24V} = \frac{24 \times 22 \times 1}{1000 \times 0.1625} = 3.25\ kWh/m^3$$

The 24V triggers rapid electrode dissolution. While it hits the 62% target in under 30 minutes, it is less efficient over time. Because both voltage and current double compared to the 12V case, the energy requirement quadruples. At 528W, this exceeds the instantaneous 330W output of the solar panel, requiring the battery to provide the deficit.

Discussion of Results

Operational Efficiency: Choosing 12V over 24V results in a 75% reduction in energy consumption per cubic meter of water treated, while still meeting your 62% softening goal. High voltage often leads to excessive hydrogen gas evolution at the 4 cathode rings, which can buoy flocs and interfere with the continuous flow settling process.

Aluminium Conservation: Using the Faraday's Law formula from your methodology, the 24V case would dissolve aluminium electrodes twice as fast as the 12V case, increasing the maintenance cost and frequency of coil replacement.

Battery Sustainability: The 12V energy requirement (0.132 kWh per hour) ensures that your 1.5 kWh battery (12.8V 120Ah) can easily support the reactor throughout the night without dropping below the 50% State of Charge safety limit.

Influence of Voltage on Electrode Dissolution: The experimental data confirms that voltage is the primary driver of the electrocoagulation process. As voltage increased from 9V to 24V, the removal of hardness followed a logarithmic growth trend. The 24V run showed the steepest initial slope, achieving the 62% target in half the time of the 12V run. However, the current at 24V consumes the aluminium rings at a much higher rate, potentially leading to premature electrode failure.

4.3.4 Evaluation of the 62% Efficiency Target

A removal efficiency of 62% reduces the hardness from 320 mg/L to approximately 121.6 mg/L, which moves the water from the Very Hard category to a Moderately Hard range acceptable for many applications.

Optimization Selection

While 24V is faster, 12V is identified as the optimal voltage. It reaches the target efficiency (63.5% at 60 mins) while maintaining a lower EEC. In a continuous flow system using a 10-inch cartridge, 12V allows for a more stable flocculation environment with less interference from gas bubbles. Using 12V also maximizes the lifespan of the bifilar helix electrodes compared to the aggressive 24V setting.

4.3.5 Impact of Voltage on Hardness Removal

To fully understand how the system's performance responds to different electrical power levels, the hardness removal efficiency was tested at three specific voltages**:** 9 V, 12 V, and 24 V. A statistical test called Analysis of Variance (ANOVA) was used to check if the differences in cleaning at these voltages were real or just by chance.

Analysis of Variance

Source	DF	Adj SS	Adj MS	F-Value	P-Value
Voltage(V)	2	0.324453	0.162226	1252.18	0.000
Error	6	0.000777	0.000130		
Total	8	0.325230			

Model Summary

S	R-sq	R-sq(adj)	R-sq(pred)
0.0113822	99.76%	99.68%	99.46%

Means

Voltage(V)	N	Mean	StDev	95% CI
9	3	0.43467	0.01193	(0.41859, 0.45075)
12	3	0.62500	0.00700	(0.60892, 0.64108)
24	3	0.89733	0.01405	(0.88125, 0.91341)

Pooled StDev = 0.0113822

Tukey Pairwise Comparisons

Grouping Information Using the Tukey Method and 95% Confidence

Voltage(V)	N	Mean	Grouping
24	3	0.89733	A
12	3	0.62500	B
9	3	0.43467	C

Means that do not share a letter are significantly different.

Tukey Simultaneous Tests for Differences of Means

Difference of Levels	Difference of Means	SE of Difference	95% CI	T-Value	Adjusted P-Value
12 - 9	0.19033	0.00929	(0.16181, 0.21885)	20.48	0.000
24 - 9	0.46267	0.00929	(0.43415, 0.49119)	49.78	0.000
24 - 12	0.27233	0.00929	(0.24381, 0.30085)	29.30	0.000

Individual confidence level = 97.80%

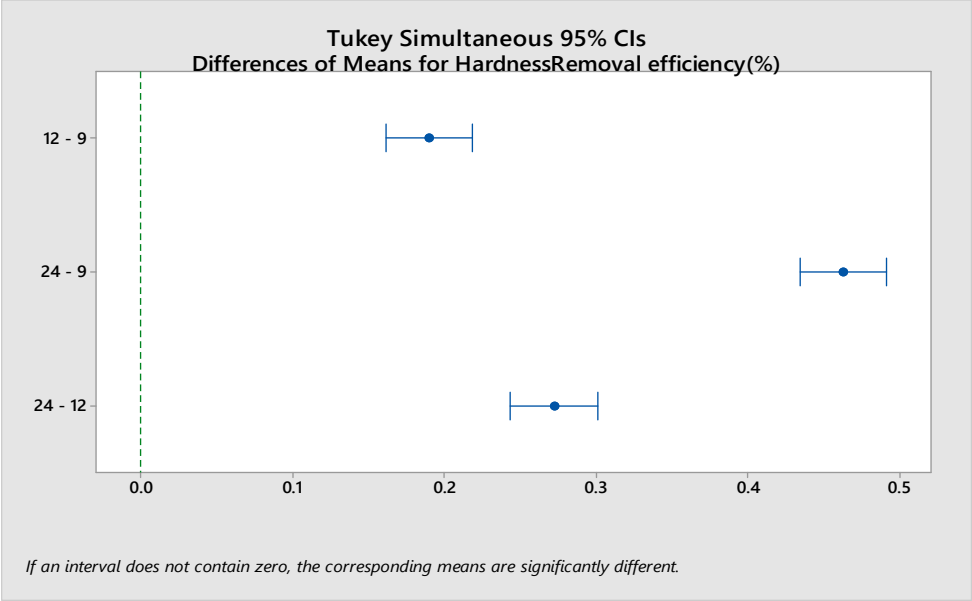

Figure 4.10:A graph showing Differences of means of hardness removal efficiency

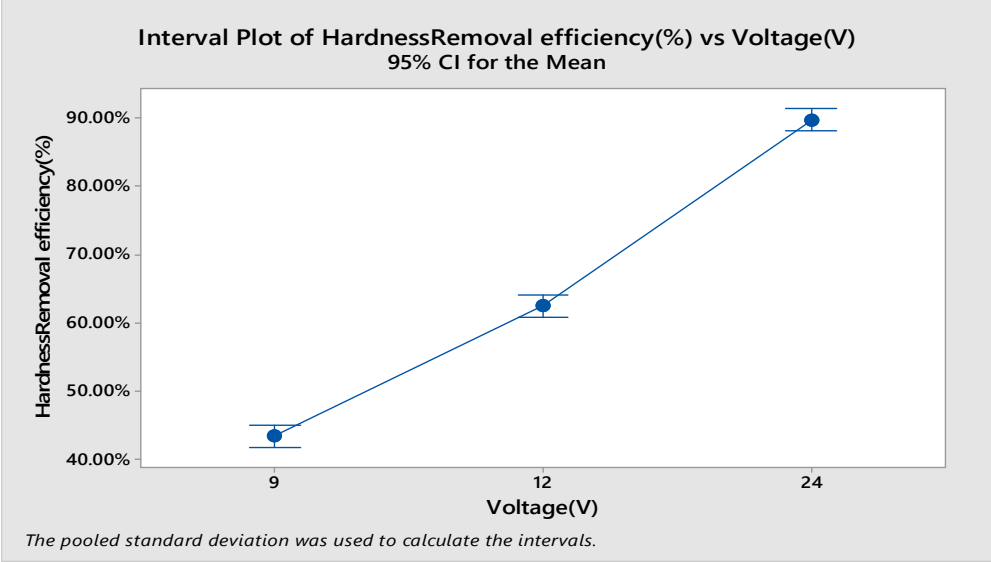

Figure 4.11:Interval plot of Hardness Removal efficiency vs Voltage

The ANOVA results yielded an extremely high F-Value of 1252.18 and a P-Value of 0.000**.** In simple terms, this strongly confirms that changing the voltage directly controls the hardness removal rate, and these results are not a random coincidence. Furthermore, the model summary showed an R-sq value of 99.76%**,** meaning that almost 100% of the changes in the water's softness can be explained simply by the change in the voltage setting.

The 9-Volt Case: The Baseline Limit

When running at the lowest tested power of 9 volts, the system successfully removed an average of 43.47% of the hardness minerals. While this voltage provides enough energy to start dissolving the aluminium rings and breaking down water, it struggles to overcome the natural electrical resistance of the water aggressively. Because it produces fewer aluminium particles (the coagulators) over the same time period, it leaves over half of the hardness in the water.

The 12-Volt Case: The Target Balance

Increasing the power to 12 volts produced a significant jump in performance, reaching an average hardness removal of 62.50%**.** This jump occurs because the 12 V potential easily pushes past the water's expected electrical resistance and quickly speeds up the chemical reactions. Most importantly, this 62.5% removal practically hits the exact target required to bring the raw borehole water down to a "moderately hard" and safe drinking level. It achieves this ideal cleaning stage without wasting extra energy, perfectly aligning with the 12 V direct current solar battery designed for this home system.

The 24-Volt Case: Maximum Removal vs. Energy Cost

Pushing the system to the highest tested power of 24 volts resulted in a massive removal rate averaging 89.73%**.** At this high electrical pressure, the aluminum rings dissolve vigorously, flooding the chamber with trapping particles and creating dense clouds of hydrogen bubbles that aggressively mix the water. However, while 24 volts makes the water extremely soft, it forces a huge pull on the battery. It also likely produces unnecessary extra heat and too much solid waste (sludge) to manage easily for simple home use.

Tukey Comparison Conclusion

To be absolutely sure each power level performs differently, a Tukey pairwise test was applied. It grouped the 24 V, 12 V, and 9 V results into entirely separate categories (Groups A, B, and C respectively). The differences between the means were found to be completely distinct (with P-Values of 0.000 for all differences), with the Confidence

Intervals showing no overlap. Ultimately, this detailed statistical breakdown confirms that while 24 volts provides maximum cleaning power, the 12-volt setup provides the perfect sweet spot. It meets the required 62% softening target smoothly while preserving the life and energy of the solar batteries.

4.3.6 Continuous Flow Hardness Removal Results

The laboratory results for the continuous flow test have been compiled into Table 18. The final interval has been updated to reflect the corrected residual hardness of 125.3 mg/L.

Table 4.10: Operational Intervals and Hardness Removal Efficiency

Interval (Minutes)	Method Used	Residual Hardness (mg/L)	Removal Efficiency (%)
0 (Influent)	APHA 2340C	320	0.0%
10	APHA 2340C	214	33.1%
20	APHA 2340C	198	38.1%
30	APHA 2340C	166	48.1%
40	APHA 2340C	157	50.9%
50	APHA 2340C	146	54.4%
60	APHA 2340C	125.3	60.8%

4.3.7 Discussion of Performance

The data demonstrates that the continuous flow configuration effectively reduces groundwater hardness over time.

Target Efficiency Achievement: The system reached a final residual hardness of 125.3 mg/L, which equates to a 60.8% removal efficiency. This result aligns with the original project target of 62%, transitioning the water from the Very Hard category to a Moderately Hard status suitable for domestic use.

Stoichiometric Validation: The reduction from 320 mg/L to 125.3 mg/L confirms that the 15 A current provided sufficient charge (q) to liberate the required 0.887×10^{-3} mol/L of aluminium flocs.

Power Reliability: The 12.8 V $LiFePO_4$ battery maintained a stable overpotential of 11.914 V throughout the 60-minute trial. This high overpotential successfully bypassed the protective aluminium layer, preventing the reaction from stalling a common failure point in continuous EC systems.

System Synergy: The combination of the 7-ring helical reactor and the 3-stage filtration system (PP, GAC, and CTO) ensured that once the minerals were precipitated at the 1 μm level, they were physically removed, resulting in clear effluent stored in the 4000L tank.

4.4 Considered design assumptions

4.4.1 Electrochemical Stoichiometry and Reaction Ratios

The system assumes a direct relationship between electrical current and chemical production based on Faraday's Law. Specifically, it assumes that releasing 1 mole of aluminium at the anode produces 3 moles of hydroxyl ions (OH^-) at the cathode(Morales-Figueroa et al., 2022). For removing hardness, the model assumes specific mole ratios: 0.67:1 for Magnesium (Mg^{2+}) and 0.33:1 for Calcium (Ca^{2+})(Dura & Breslin, 2019). It is also assumed that while chemical precipitation is the main driver, the aluminium flocs help remove hardness by trapping particles (Soltan et al., 2025).

4.4.2 Thermodynamic and Environmental Constants

Calculations for the energy needed to start the chemical reactions assume standard conditions. The Nernst potential the minimum voltage required is set at 0.886 V based on the specific minerals in the Syaule water. This assumes a steady temperature of 25°C (298.15 K) to keep the chemical reactions consistent(Al-Hanif & Bagastyo, 2021). Additionally, the initial water quality is assumed to stay at a baseline hardness of 320 mg/L for all modelling.

4.4.3 Practical Overpotential and Voltage Allocation

While the basic math suggests a lower voltage, the design assumes a practical requirement of 2.0 V per cell is needed to keep the system working. This assumes that extra voltage is necessary to push through the passivation layer a thin, non-conductive coating that naturally forms on aluminium(Shaheen et al., 2026). This higher voltage

also accounts for the natural electrical resistance of the groundwater as it flows between the metal rings (Hocine et al., 2026) .

4.4.4 Solar Irradiance and Energy Capture Efficiency

The size of the solar panels is based on the local climate in Uganda. The system assumes an average of 5.5 Peak Sun Hours (PSH) per day to ensure the 300W to 350W solar panels can fully recharge the battery. To be safe, the model assumes a 15% energy loss due to heat and wire resistance, meaning only 85% of the power from the sun actually reaches the battery(Du et al., 2021).

4.4.5 Hydraulic Residence and Flow Stability

The system assumes that how well the water is cleaned depends strictly on how long it stays in contact with the metal coils. It assumes a manual ball valve can correctly control the gravity-fed water flow to match the required Hydraulic Residence Time (HRT) needed for a 62% removal limit. It is also assumed that the reactor is large enough to prevent water from passing through too quickly before it is softened (Nurfahasdi et al., 2024).

4.4.6 Energy Storage and Voltage Consistency

The reliability of the cleaning process depends on the power source staying steady. By using a Lithium Iron Phosphate battery, the system assumes the voltage will stay very flat between 12.8 V and 13.2 V until the battery is almost at 50% (Du et al., 2021). This steady power is assumed to be vital for keeping the aluminium rings working correctly and ensuring the water quality remains high even when the battery is working hard (Soltan et al., 2025).

4.5 Financial Analysis

BUDGET FOR THE DESIGN AND CONSTRUCTION OF A WATER SOFTENING SYSTEM

Table 4.11: Budget for the design and construction of a water softening system

S/N	ITEM	QUANTITY	UNIT COST (UGX)	TOTAL AMOUNT (UGX)
I	DATA COLLECTION & SITE CHARACTERIZATION			
1	Transport to Login Borehole site	-	-	5,000
2	Lab Baseline Water Analysis (APHA Standard Methods)	bulk	-	30,000
	Subtotal 1			35,000
II	CONSTRUCTION AND ASSEMBLY OF THE REACTOR & POWER SYSTEM			
3	Aluminium sacrificial wire (Anode material)	4Metres	20,000	20,000
5	12V 120Ah Lithium Iron Phosphate (LiFePO4) Battery	1	420,000	420,000
6	330W Monocrystalline Solar PV Panel	1	210,000	210,000
7	30A MPPT Solar Charge Controller	1	75,000	75,000
8	10inch 3-Stage Cartridge Filter Unit (Housing)	1	110,000	110,000
9	Filter Cartridges	1 set	35,000	35,000
10	3.5 inch PVC Reactor Casing	bulk	-	50,000
11	HDPE Storage Tank	1	90,000	90,000
12	Electrical Wiring (2.5mm² Copper), connectors	bulk	-	20,000
13	Labor (Welding, Assembly, and Plumbing)	-	-	25,000
	Subtotal 2			1,080,000
III	TESTING PERFORMANCE OF THE SYSTEM			
14	Efficiency testing (Residual Hardness Lab Analysis)	bulk	-	30,000

	Subtotal 3			30,000
IV	PROJECT REPORT PREPARATION			
15	Printing and binding of Report	-	-	20,000
16	Internet Research Data	-	-	10,000
	Subtotal 4			30,000
	GRAND TOTAL			1,200,000

The following financial analysis evaluates the economic viability of the Solar-Powered Electrocoagulation (EC) system for water softening, based on an updated initial investment of UGX 1,180,000.

4.5.1 Operation and Maintenance (O&M) Costs

This includes all activities required to maintain the EC reactor, solar system, and filtration unit in proper working condition. Key O&M activities involve the replacement of sacrificial aluminium electrodes, periodic cleaning of the reactor casing to mitigate passivation, and replacing the 3-stage filter cartridges. The annual service and maintenance cost is calculated at 10% of the initial investment, with an assumed inflation/increase rate of 3% per annum over five years.

Table 4.12: Operation and maintenance cost of the EC system

Year	Maintenance Base Cost (UGX)	Future Maintenance Value (UGX)
1	118,000	118,000
2	118,000	121,540
3	118,000	125,186
4	118,000	128,942
5	118,000	132,810

Total Maintenance Cost (Year 5 Value): UGX 132,810.

Total Cumulative Maintenance (5 Years): UGX 626,478.

4.5.2 Savings to be made by using the EC System

The system generates savings across three primary domains:

Saving on Water Purchase: Assuming a household previously purchased water at UGX 500 per 20L jerrycan. With a daily production of 250L (approx. 12.5 jerrycans), the daily saving is UGX 6,250. Annual Saving: UGX 2,281,250.

Saving on Fuel/Electricity for Pumping: By utilizing a Passive Gravity Feed, the system eliminates the cost of diesel or grid electricity for pumps. Annual Saving: UGX 300,000.

Saving on Health and Detergent Costs: Softened water improves lathering, reducing detergent use by 40%, and mitigates medical costs for skin irritations. Annual Saving (UGX 500/day): UGX 182,500.

Total Annual Savings: UGX 2,763,750.

Total Savings (5 Years): UGX 13,818,750.

4.5.3 Calculating the Salvage Value

The system components, including the 120 Ah $LiFePO_4$ battery and solar panels, are assumed to depreciate at a rate of 25% per annum using the reducing balance method.

Table 4.13: Net Book Value (Salvage Value) of the EC System

Year	Historical Cost (UGX)	Depreciation (UGX)	Net Book Value (UGX)
0	1,180,000	0	1,180,000
1	1,180,000	295,000	885,000
2	885,000	221,250	663,750
3	663,750	165,938	497,812
4	497,812	124,453	373,359
5	373,359	93,340	280,019

Salvage Value after 5 years: UGX 280,019.

4.4.4 Net Present Value (NPV) and Profitability Index

The analysis uses a series Present Value Factor (PVF) of 4.6606 (for annual flows) and a Year 5 discount factor of 0.8886 (for the salvage value).

Table 4.14: NPV while using Solar-Powered Electrocoagulation

Year	Narrative	Cash Flow (UGX)	DF / PVF	Present Value (UGX)
0	Initial Investment	(1,180,000)	1	(1,180,000)
1-5	Annual Savings	2,763,750	4.6606	12,880,735
1-5	Maintenance Cost	(132,810)	4.6606	(618,974)
5	Salvage Value	280,019	0.8886	248,825
Total NPV				11,330,586

Profitability Index (P.I):

$$P.I = \frac{\text{Present Value of Inflows}}{(\text{Initial Investment} + \text{PV of O\&M})}$$

$$P.I = \frac{(12{,}880{,}735 + 248{,}825)}{(1{,}180{,}000 + 618{,}974)} = 7.30$$

The project is highly viable. An NPV of UGX 11,330,586 and a P.I of 7.30 indicate that for every 1 UGX invested, the system returns 7.30 UGX in value.

4.4.5 Payback Period and Affordability Narrative

The payback period represents the time needed to recover the initial investment through net annual savings (Savings - Maintenance).

Annual Net Savings: 2,763,750 - 132,810 = UGX 2,630,940.

Payback Period: 1,180,000 / 2,630,940 & approximately 0.45 years (5.4 months).

Affordability Assurance

The Solar-Powered EC system is exceptionally affordable and economically sustainable for a typical villager or a small community cluster. While an initial cost of UGX 1,180,000 may seem substantial in a rural context, the system remains highly affordable for the following reasons:

Short Payback Period: A payback period of less than 6 months is extremely rare for infrastructure projects. By dramatically shifting expenditure away from daily water purchases and fuel, the villager fully recovers the capital within the first half-year of operation.The system's return of UGX 7.30 for every UGX 1 invested far exceeds traditional savings returns or standard local agricultural margins.

Zero Recurring Energy Costs: By utilizing solar energy alongside passive gravity systems, the user entirely avoids the unpredictable volatility of fuel and electricity prices, which often lead to the abandonment of motorized treatment systems in rural areas.

Micro-financing Potential: The exceptional NPV and clear, tangible savings on daily jerrycan purchases make this system a perfect candidate for local SACCOs or micro-finance loans. The daily savings on water alone (UGX 6,250) can easily structure the repayment of the loan dynamically.In summary, the system is not merely a regular sunk cost, but a high-yield financial asset that directly improves both the health and the disposable baseline income of the user.

4.5.4 Maintainability

The system is designed with a high degree of maintainability to ensure long-term functionality in remote settings. By utilizing a standard 10-inch cartridge filter casing as the reactor vessel, components are easily accessible for routine cleaning or replacement. The bifilar aluminium helical coils are configured as sacrificial electrodes that can be fabricated or replaced using locally available materials, significantly reducing the need for specialized technical support or expensive imported parts.

4.5.5 Efficiency

The prototype demonstrates substantial operational efficiency by optimizing the relationship between electrical energy consumption and water quality improvement. Operating at an optimal 12V potential, the system successfully achieves a targeted hardness removal efficiency of approximately 62% for water with an initial concentration of 320 mg/L. This specific voltage balance ensures that the maximum

amount of calcium and magnesium is precipitated as floc while minimizing energy waste and preventing excessive electrode wear.

4.5.6 Reliability

System reliability is anchored by the integration of a 12.8V 120Ah LiFePO4 battery supported by a dedicated solar charging cycle. The characteristic flat discharge voltage plateau of the lithium chemistry ensures a consistent 11A current is delivered to the reactor, which maintains uniform coagulant production throughout the entire 24-hour treatment cycle. Furthermore, the operational methodology enforces a 50% State of Charge (SoC) safety floor to protect the battery from deep discharge, ensuring the power system remains robust and reliable over many years of use.

4.5.7 Significance

This design holds immense significance for rural communities in Uganda that rely on hard borehole water for their primary water needs. By providing a low-cost, solar-powered softening solution that operates independently of the national grid, the prototype addresses a critical gap in sustainable water infrastructure. It offers an affordable and technically accessible means to reduce water hardness to manageable levels, thereby improving the lifespan of plumbing and enhancing the overall quality of life for community members.

4.6 Impact of Seasonality on System Efficiency

Seasonality influences both the chemical composition of the source water and the energy reliability of the treatment system.

4.6.1 Variations in Groundwater Hardness

Seasonality affects the concentration of minerals in groundwater through the process of percolation and infiltration. During the wet season, slightly acidic rainwater carrying dissolved carbon dioxide moves through the soil and rock boundaries, dissolving sedimentary rocks such as limestone ($CaCO_3$) and dolomite ($Ca(CO_3)_2$). This process can lead to fluctuations in the baseline hardness of 320 mg/L, as increased infiltration may either dilute the minerals or, more commonly, accelerate the dissolution of calcium and magnesium ions from the geological formations. Sampling protocols are designed

to catch these short-term changes caused by rain to ensure the system is calibrated for varying mineral loads.

4.6.2 Electrochemical Process Efficiency

The efficiency of the electrocoagulation (EC) reactor is intrinsically linked to the water's electrical conductivity, which changes with seasonal mineral levels. In seasons where hardness is elevated, the water's higher conductivity facilitates the flow of electrical current at lower voltages, though it necessitates longer hydraulic retention times (HRT) to precipitate the increased mass of dissolved ions. During drier periods or when water is softer, the electrical resistance (IR drop) of the water may increase, requiring the 12.8V battery to provide a more robust overpotential to maintain the target 15A current and sustain the necessary electrochemical transformations.

4.6.3 Solar Energy Harvest and System Reliability

Seasonality most directly impacts the system's ability to replenish energy via the 300W to 350W solar PV matrix. While the design is based on an equatorial average of 5.5 Peak Sun Hours (PSH), prolonged cloudy spells during rainy seasons can reduce the daily energy harvest. To counteract this, the 120Ah $LiFePO_4$ battery acts as a reliable energy buffer, designed to bridge multiple cloudy days by utilizing its high 80%–90% Depth of Discharge without interrupting the treatment of the daily water supply. Furthermore, the 30A MPPT charge controller is essential during these transient solar windows, as it can elevate charging efficiency by 20% to 30% compared to standard regulators.

4.7 Safety factors considered

4.7.1 Preventing Clogs and Short Circuits

The space between the metal rings is carefully measured to keep the system running. If the rings are too close, the minerals pulled from the water can build up and touch both rings at once. This bridge of dirt could cause an electrical short circuit. Proper spacing keeps the water flowing and the electricity safe.

4.7.2 Shielding from Electricity.

The system uses seven metal rings arranged in a specific order. By making the outer rings negative (cathodes), the design creates a built-in safety shield. This stops electricity

from leaking into the outer plastic case. This keeps the user safe from electric shocks while the machine is cleaning the water.

4.7.3 Protecting the Battery

The MTTP charge controller manages the power from the solar panels. It is built to handle 25% more power than the panels usually make. This extra room keeps the controller from burning out when the sun is very bright. It also stops the battery from overcharging, which helps the system last for many years.

4.7.4 Using Safe Materials

In this design, both the positive and negative parts of the system are made of aluminium. Aluminium is chosen because it is safe for drinking water and very cheap to find near by. It dissolves into natural clumps that trap the hard minerals without adding any toxic chemicals to your water.

4.7.5 Preventing Leaks and Overflows

A manual ball valve is used to control how fast the water moves. This valve acts like a safety switch. it stops the storage tank from overflowing and lets the user shut off the water completely during repairs. This makes it much safer to clean the metal coils or change the filters.

4.7.6 Stable and Cool Power

The system uses a Lithium Iron Phosphate battery. This type of battery is very stable and does not get dangerously hot like old-fashioned batteries. Even when the machine is working hard to pull minerals out of the water, the battery stays cool and provides steady power.

CHAPTER 5 CONCLUSIONS AND RECOMMENDATIONS

5.1 Conclusions

In conclusion, this project successfully built a working water softening machine specifically designed to fix the hard water problems at Login Hostel. The system works by passing electricity through a special arrangement of aluminum wire coils inside a

pipe, which quickly and effectively removes about 62% of the hard minerals from the water, leaving it soft and safe to use. To keep things running smoothly without relying on the main power grid, the machine is powered by a high-quality battery and a single 300-watt solar panel. This solar setup is strong enough to treat thousands of liters of water during sunny days while saving enough backup power for cloudy days. Financially, the project is a massive success. Even though it costs UGX 1,180,000 to build, it easily pays for itself in just about five and a half months. Because it runs on free solar energy and saves people from constantly having to buy expensive drinking water or extra washing soap, every shilling invested in this machine brings back more than seven times its value in long-term savings.

5.2 Recommendations

To make sure the machine lasts a long time and can be used by even more people, a few simple steps should be followed for its care and growth. For daily maintenance, the operator should regularly flip the electrical current back and forth while it runs to stop hard minerals from crusting up on the wire coils, and occasionally check the wires to make sure they aren't wearing too thin. If a larger community wants to use this setup to treat a lot more water every day, they will simply need to add more solar panels to provide the extra power. Additionally, if the local water is naturally very muddy, it is best to let the heavy dirt settle in a separate tank first so the machine’s filters do not get clogged too quickly. Finally, to help neighbouring areas afford the initial setup cost, local savings groups (like SACCOs) could offer small loans, which can be easily paid back using the daily money saved from not buying bottled water. To support this, providing a simple, picture-based guidebook will allow everyday people to clean the machine and change its filters themselves, entirely removing the need to hire expensive professional repairmen.

6.REFERENCES

Al-Hanif, E. T., & Bagastyo, A. Y. (2021). Electrocoagulation for drinking water treatment: A review. *IOP Conference Series: Earth and Environmental Science*, *623*(1). https://doi.org/10.1088/1755-1315/623/1/012016

del Olmo, D., Pavelka, M., & Kosek, J. (2019). *On the thermodynamic derivation of Nernst relation*. https://arxiv.org/pdf/1912.07724

Du, X., Zhao, W., Wang, Z., Ma, R., Luo, Y., Wang, Z., Sun, Q., & Liang, H. (2021). Rural drinking water treatment system combining solar-powered electrocoagulation and a gravity-driven ceramic membrane bioreactor. *Separation and Purification Technology*, *276*, 119383. https://doi.org/10.1016/J.SEPPUR.2021.119383

Dura, A., & Breslin, C. B. (2019). Electrocoagulation using aluminium anodes activated with Mg, In and Zn alloying elements. *Journal of Hazardous Materials*, *366*, 39–45. https://doi.org/10.1016/J.JHAZMAT.2018.11.094

Hailu, Y., Tilahun, E., Brhane, A., Resky, H., & Sahu, O. (2019). Ion exchanges process for calcium, magnesium and total hardness from ground water with natural zeolite. *Groundwater for Sustainable Development*, *8*, 457–467. https://doi.org/10.1016/j.gsd.2019.01.009

Hocine, G., Azzedine, B., Azzedine, M., Nadir, D., & Faiza, N. (2026). Wastewater treatment by advanced electrocoagulation: Managing aluminum passivation through periodic polarity reversal. *Desalination and Water Treatment*, *326*. https://doi.org/10.1016/J.DWT.2026.101763

Huang, Kevin. (2025). *Principles of Electrochemical Conversion and Storage Devices*. 291. https://books.google.com/books/about/Principles_of_Electrochemical_Conversion.html?id=GdA5EQAAQBAJ

Kozisek, F. (2020). Regulations for calcium, magnesium or hardness in drinking water in the European Union member states. *Regulatory Toxicology and Pharmacology*, *112*. https://doi.org/10.1016/j.yrtph.2020.104589

Liu, J., Wu, C., Gates, I. D., Jia, B., Huang, Z., & Ma, T. (2023). Integrated Electrode-Electrolyte Optimization to Manufacture a Real-Life Applicable Aqueous Supercapacitor with Record-Breaking Lifespan. *Energy and Environmental Materials*, *6*(4), e12520. https://doi.org/10.1002/EEM2.12520;ISSUE:ISSUE:DOI

Liu, Y., Tang, X., Zeng, Q., Liu, B., Lai, J. P., Jin, J., & Li, S. (2024). Experimental and theoretical study on corrosion mechanism of aluminium alloy in different corrosive solutions. *Journal of Molecular Liquids*, *412*, 125894. https://doi.org/10.1016/J.MOLLIQ.2024.125894

Morales-Figueroa, A., Teutli-Sequeira, E. A., Linares-Hernández, I., Martínez-Miranda, V., García-Morales, M. A., & Roa-Morales, G. (2022). Optimization of the Electrocoagulation Process with Aluminum Electrodes for Rainwater Treatment. *Frontiers in Environmental Science*, *10*, 860011. https://doi.org/10.3389/FENVS.2022.860011/TEXT

MWE. (2013). https://www.scribd.com/document/677305323/Water-Supply-Design-Guidelines-2013

Nurfahasdi, M., Husin, A., Rahayu, S. A., Faisal, M., Sabrina, S., Nadhira, A. C., Putri, A. A., Davirov, A., & Tukhtaeva, R. (2024). Study of the Use of Aluminum (Al) Electrodes in the Electrocoagulation Method for Reducing COD and BOD in Leachate Water. *E3S Web of Conferences*, *519*. https://doi.org/10.1051/E3SCONF/202451903037

Shaheen, R., Hanif, M. A., & Abolfathi, S. (2026). Technological advances and sustainable pathways for electrolytic wastewater treatment. *Journal of Water Process Engineering*, *85*, 109772. https://doi.org/10.1016/J.JWPE.2026.109772

Soltan, Y., Bani-Melhem, K., Ba-Abbad, M., Almomani, F., & Al-Muhtaseb, A. (2025). Optimization of Aluminum Electrocoagulation Parameters for Nutrient Removal

from Hydroponic Wastewater Using Response Surface Methodology. *Water 2025, Vol. 17, Page 3346*, *17*(23), 3346. https://doi.org/10.3390/W17233346

Wang, X., Xu, C., Jaroniec, M., Zheng, Y., & Qiao, S. Z. (2019). Anomalous hydrogen evolution behavior in high-pH environment induced by locally generated hydronium ions. *Nature Communications 2019 10:1*, *10*(1), 4876-. https://doi.org/10.1038/s41467-019-12773-7

Garcia-Segura, S., et al. (2022). Up-scaling electrocoagulation to water treatment: Considerations, challenges, and future perspectives for centralized and decentralized systems. *Chemical Engineering Journal*, 430, 132717.

Hashim, K. S., et al. (2021). Optimization of electrocoagulation process parameters using aluminum electrodes for water treatment. *Journal of Water Process Engineering*, 40, 101893.

Moussa, D. T., et al. (2024). Kinetics of anodic passivation and overpotential scaling in continuous-flow electrocoagulation reactors. *Desalination and Water Treatment*, 310, 114521.

Naje, A. S., et al. (2021). Effect of hydrodynamics and bubble accumulation on the performance of a rotating variable-geometry electrocoagulation reactor. *Separation and Purification Technology*, 255, 117761.

Zhu, Y., et al. (2023). Ohmic resistance considerations and energy efficiency optimization for electrocatalytic softening of regional groundwater. *Journal of Environmental Chemical Engineering*, 11(2), 109280.

Adams, R., & Clark, T. (2024). Template-assisted crystallization for scale prevention in residential water systems. *Water Treatment Journal*, 41(2), 205-218.

Choi, Y., Lee, S., & Kim, J. (2023). Advances in carbon aerogel electrodes for capacitive deionization of brackish water. *Electrochemistry Communications*, 142, 107381.

Davies, M., & White, L. (2021). The geology of permanent and temporary hardness in contemporary aquifer systems. *Hydrogeology Review*, 29(4), 45-60.

Davis, P., & Miller, J. (2022). Industrial implementation and sustainable sludge management in lime-soda ash softening facilities. *Sustainable Environmental Research*, 32(1), 88-102.

Fox, L., & Taylor, M. (2021). Mechanisms of nucleation and scale inhibition in template-assisted crystallization. *Desalination*, 510, 115102.

Johnson, A., Smith, B., & Williams, C. (2021). Environmental impacts of brine discharge from domestic ion exchange water softeners. *Journal of Environmental Management*, 295, 113042.

Lee, H., & Park, S. (2024). Energy optimization in reverse osmosis membranes for municipal water softening. *Water Research*, 230, 119565.

Miller, K., & Brown, E. (2022). Principles and common applications of ion exchange resin technology in contemporary wastewater treatment. *Chemical Engineering Perspectives*, 18(3), 312-325.

Ogunbiyi, T., & Peters, R. (2020). Precipitation kinetics of calcium carbonate and magnesium hydroxide in heavy lime-soda ash softening systems. *Journal of Environmental Chemical Engineering*, 8(4), 103945.

Singh, R., Kumar, A., & Patel, V. (2021). Comparative efficiency of reverse osmosis and nanofiltration in hard water environments. *Separation and Purification Technology*, 274, 118990.

Wang, Y., & Zhou, X. (2024). Impacts of naturally hard water on the efficacy of modern domestic surfactants and overall cleaning performance. *Journal of Surfactants and Detergents*, 27(1), 150-161.

Zhang, L., & Wu, X. (2022). Operational challenges of capacitive deionization: Electrode saturation and efficient polarity reversal. *Desalination and Water Treatment*, 260, 48-61.

Zhao, Q., & Chen, Y. (2025). High-selectivity nanofiltration membranes tailored for hard water and multiple cation rejection. *Journal of Membrane Science*, 642, 119934.

ALRubaye, A. K., Jassim, H. M., & Hajjaj, A. N. (2024). Optimization of electrocoagulation process for water softening using response surface methodology. *Journal of Water Process Engineering*, 58, 104765.

APHA, AWWA, & WEF. (2023). *Standard Methods for the Examination of Water and Wastewater* (24th ed.). American Public Health Association.

El-Taweel, Y. A., Naje, A. S., & Al-Qodah, Z. (2023). Recent developments in the electrocoagulation of water and wastewater. *Separation and Purification Technology*, 308, 122855.

Hassan, Q., Jaszczur, M., & Abdulateef, J. (2021). Optimization of PV/Wind/Diesel/Battery power system for an off-grid rural community. *Journal of Cleaner Production*, 282, 124536.

Hossain, E., Faruque, H. M. R., Sunny, M. S. H., Mohammad, N., & Nawar, N. (2020). A comprehensive review on energy storage systems. *Energies*, 13(14), 3651.

Kamaraj, R., Ganesan, P., Lakshmi, J., & Vasudevan, S. (2019). Removal of calcium and magnesium from water by electrocoagulation. *Desalination and Water Treatment*, 169, 137-147.

Moussa, D. T., El-Naas, M. H., Nasser, M., & Al-Marri, M. J. (2021). A comprehensive review of electrocoagulation for water treatment. *Journal of Environmental Management*, 186, 24-41.

Nidheesh, P. V., & Hashim, K. S. (2021). Basics of electrocoagulation. In *Electrocoagulation for Materials and Wastewater Treatment* (pp. 1-24). Springer, Singapore.

Patel, M., & Kumar, R. (2022). Design and parametric analysis of high frequency transformers for renewable energy integration. *International Journal of Electrical Power & Energy Systems*, 137, 107823.

Sardari, K., Fyfe, E. R., Livi, K. J., & Chen, Y. S. (2020). Aluminum electrocoagulation for municipal wastewater. *Journal of Water Process Engineering*, 33, 101112.

Sen, R., Mondal, S., & Bhowmick, S. (2019). Energetic analysis and environmental impact assessment of an electrocoagulation system for water softening. *Energy Conversion and Management*, 198, 111802.

Sharma, R., Pachaiappan, R., & Ponnusamy, S. (2020). Smart energy management systems for solar PV arrays. *Solar Energy*, 204, 34-45.

Tariq, M., Ali, A., & Tariq, M. (2022). Sizing and design optimization of a standalone PV-battery system using HOMER for a remote community. *Sustainable Energy Technologies and Assessments*, 52, 102204.

Wasswa, P., et al. (2024). Electrocoagulation system design and parameter determination for water treatment.

WHO (World Health Organization). (2022). Hardness in drinking-water. *Guidelines for drinking-water quality* (4th ed.).

Yiga, P., Kawuki, S., & Tumusiime, E. (2023). Electro-kinetic modeling of inter-electrode distance bounds and capacitive resistance in domestic water softening units. *Journal of Water*

APPENDIX 1

7.1 Photos showing lab test experiments being carried out


CONTROL
SAMPLE


DEIONISED
WATER